IEEE Access
Multidisciplinary : Rapid Review : Open Access Journal

Received 16 July 2025, accepted 2 September 2025, date of publication 4 September 2025, date of current version 11 September 2025.

Digital Object Identifier 10.1109/ACCESS.2025.3606339

RESEARCH ARTICLE

Real-Time Activity Recognition Using Minimal Biomechanical Features: A Lightweight IMU-Based Classifier for Older Adults

EHSAN SHARAFIAN M., COLBY ELLIS, AND BABAK HEJRATI

Department of Mechanical Engineering, The University of Maine, Orono, ME 04469, USA

Corresponding author: Babak Hejrati (babak.hejrati@maine.edu)

This work was supported by the National Science Foundation (NSF) under Grant 2145177.

This work involved human subjects or animals in its research. Approval of all ethical and experimental procedures and protocols was granted by the University Institutional Review Board at the University of Maine under Application No. 2019-04-15.

ABSTRACT Real-time implementation of human activity recognition systems is often challenging due to high computational costs and the need for extensive datasets. Existing models rarely account for older adults, particularly those with mobility limitations. This study proposes a lightweight classifier for redhuman activity recognition that utilizes minimal biomechanical features based on thigh and foot angles measured by two IMUs to classify activities, including walking, stair ascent and descent, standing, and sitting. Data from 10 young adults were used to train the model, which was subsequently tested on separate cohorts of 5 young and 10 older adults. A KNN classifier was implemented in a smartphone application for real-time use. To optimize its performance, an adaptive segmentation method was developed to accurately detect toe-off in different activities and reduce computational overhead. The model was trained to recognize mobility limitations in older adults, non-alternating leg stair negotiation, where individuals rely on one leg. redRather than using deep learning architectures, the proposed physics-based framework uses simple and interpretable biomechanical features to enable real-time implementation on resource-constrained devices. The system achieved overall 99% detection accuracy for young and old adults with normal movement patterns and achieved 93% accuracy in distinguishing non-alternating leg stair negotiation from normal stair negotiation patterns in older adults. The results demonstrate the feasibility of a computationally efficient model with minimal features for real-time applications. By addressing the movement characteristics of older adults, this study contributes to the development of an accessible health monitoring system for real-world activity detection in aging populations.

INDEX TERMS Adaptive windowing, biomechanical features, human activity recognition (HAR), machine learning, older adults, non-alternating stair negotiation.

I. INTRODUCTION

Human activity recognition (HAR) is considered a wide range of applications, including assisted living, medical, and healthcare [1], rehabilitation [2], smart homes [3], and industrial settings as a system for human-machine interactions. HAR systems aim to automatically identify and analyze human activities using data from wearable sensors or camera-based technologies, where in the context of assisted living, implementing wearable sensors can lead to a healthier lifestyle and independence for people [4]. The monitoring and classification of daily activities are crucial to assessing the quality of life for different age groups, as well as predicting potential abnormalities in movement patterns [5], [6], [7]. Furthermore, HAR systems can investigate physical activity [8] and provide feedback to motivate people to adhere to daily physical activity targets [9]. Accurate information on daily patterns can improve the treatment and diagnosis

The associate editor coordinating the review of this manuscript and approving it for publication was Jingang Jiang.

of neurological and respiratory disorders, particularly for older adults [4]. HAR is also a valuable tool in the field of Ambient Assisted Living (AAL), offering various solutions to improve the quality of life for frail individuals and those with disabilities while enhancing health and independence [10].

Body-worn sensors are suitable for collecting data over an extended time in HAR systems. Inertial measurement units (IMUs) are often the preferred type of body-worn sensors due to their ability to provide precise and consistent measurements of motion and orientation without limitations such as blind spots or environmental dependencies [11]. Unlike camera-based systems, IMUs can be used in diverse environments and are not limited by visual obstructions or lighting conditions [12], [13]. However, IMU-based HAR systems require proper feature representation and classifiers for the collected data. A spectrogram-based feature extraction approach combined with data augmentation techniques can significantly enhance recognition accuracy. These methods address the issue of data scarcity and have been shown to produce promising results when applied to datasets such as the UCI HAR dataset [14]. Combining data from multiple IMUs placed on different body positions can further improve the HAR accuracy. An attention-based fusion mechanism can determine the significance of each sensor, leading to better feature representation and classification performance. This approach has outperformed state-of-the-art methods across various activity categories [15]. Additionally, the integration of IMUs with the Internet of Things (IoT) and machine learning (ML) techniques enables real-time monitoring and personalized activity recognition with a high accuracy of 97% in daily activity [16].

Traditional sensor-based HAR systems heavily rely on the selection of biomechanical features from IMU signals to represent human movement accurately. For instance, methods using Extreme Gradient Boosting (XGBoost) have been successful in classifying IMU-derived biomechanical features for balance assessment [17], [18]. In addition, studies have highlighted the importance of features extracted from key body segments such as thigh and foot angles for detecting transitions between activities like walking and stair negotiation [5], [19]. By focusing on these minimal yet critical features, researchers seek to reduce misclassification due to complex and noisy IMU data, highlighting the potential of physics-based feature selection in creating robust and computationally efficient HAR systems.

The integration of deep learning (DL) techniques, such as convolutional neural network (CNN), deep convolutional neural network (DCCN), and long short-term memory networks (LSTM), have shown promise in enhancing HAR systems' ability to extract spatial and temporal features, leading to better performance in health monitoring applications [6], [20], [21]. Various DL models such as CNNs, LSTMS, and Transformers have been employed to enhance HAR accuracy, focusing on feature extraction of the patterns of activities. For instance, conformer-based models and lightweight Transformers have superior performance in capturing temporal dynamics [13], [22]. Ali and Abdelhafeez [23] showed that a combination of CNN and LSTM models can enhance the accuracy and robustness of HAR systems, demonstrating the potential for real-time applications. Ordóñez and Roggen [24] investigated how recurrent architectures like LSTM can have better segmentation characteristics than a normal CNN. Combining different models and techniques, such as hybrid learning models with feature analysis and data correction, can achieve high classification accuracy. For instance, using XGboost and Convolutional Variational Autoencoder (CVAE) models has resulted in a classification accuracy of 96% for detecting standing, sitting, walking, and running [25]. Both ML and DL models have been employed for HAR using IMU's accelerometer and gyroscope data, with LSTM models achieving high accuracy scores of 99%. These models are successful in capturing the temporal dynamics of human activities [26], [27]. Tang et al. [28] proposed a deep CNN using a Hierarchical-Split (HS) block to extract multiscale features, enabling the model to learn richer representations by capturing larger receptive fields. Their method achieved high accuracy (up to 99.02%) on benchmark datasets like UCI-HAR, WISDM, PAMAP2, and UNIMIB-SHAR. Alawneh et al. [29] proposed a personalized HAR framework using LSTM models within an edge–cloud architecture to recognize 17 daily activities. Their system employed incremental learning to adapt to user-specific patterns and achieved up to 98.54% accuracy using the UniMiB SHAR dataset. Akter et al. [30] introduced a CNN-based HAR model integrating attention mechanisms (CBAM) and spectrogram features, achieving results across three benchmark datasets, including KU-HAR, with up to 96.86% accuracy.

Although combining DL models for feature extraction with ML classifiers, such as SVM, KNN, NB, and LDA has significantly improved HAR performance, several challenges remain. A major obstacle is the high computational cost, which results in considerable delays for real-time detection and often necessitates extensive datasets and multiple IMUs for accurate recognition. Furthermore, these approaches typically require powerful processing units or even the integration of additional technologies like IMU and WiFi [12] for cloud-based processing. The primary limitation with CNN, LSTM, and Transformer approaches is that their feature extraction processes are not fully optimized and require significant computational resources. As a result, the unoptimized version of them may not be a suitable approach for real-time HAR applications, and other solutions should be implemented. Physics-based features derived from human movement biomechanics could be a promising alternative. Instead of relying on deep convolutional or recurrent layers, a simplified method can be used, where biomechanical variables are directly extracted and classified using conventional ML algorithms. This approach reduces computational demands while maintaining acceptable accuracy for real-time activity recognition.

Real-time HAR systems often require low latency, efficient processing, and computational cost. Considering this, heuristic feature-based ML algorithms are suitable techniques to achieve the mentioned desired properties of a system. For example, a support vector machine with a radial basis function kernel (RBF-SVM), enhanced with spherical normalization, achieved a high accuracy of 97.35% while maintaining low latency output [31]. Zhou et al. [32] introduced a resource-efficient DeepConv LSTM model, designed specifically for edge devices using TinyML. Their model captures both spatial and temporal features, targeting real-time HAR in low-power, memory-constrained environments, which achieved an accuracy of 98.24% in recognition of the activities. Deng et al. [33] proposed a lightweight HAR framework using knowledge distillation to transfer information from deep models to compact architectures, enabling efficient and accurate activity recognition on resource-constrained wearable devices. Various classifiers have been evaluated for their effectiveness in real-time HAR applications. Studies have shown that classifiers like KNN and decision trees (DT) provide high accuracy with low computational requirements, suitable for implementation on microcontrollers in wearable devices [34], [35]. DTs, in particular, are valued for their ease of implementation and minimal resource consumption [36], [37]. Additionally, SVM with a quadratic kernel and ensemble classifiers using bagging and boosting techniques have demonstrated superior performance in HAR tasks, achieving accuracies of 93.5% and 94.6%, respectively. Logacjov et al. [38] introduced the HARTH dataset for HAR includes 12 annotated activities collected using two accelerometers. Among seven machine learning and deep learning models, SVM could reach the best accuracy with F1-score 0.81. These classifiers are further optimized by excluding less relevant features, making them lightweight and suitable for real-time applications [39].

Among studies incorporating biomechanical features for movement activity classification, thigh-related features are particularly significant, especially for distinguishing stair negotiation (SN) activities. Ansah et al. [40] used an IMU placed solely on the thigh for event-based feature extraction to detect stair ascent and descent, including their transition moments to level walking. Cheng et al. [41] utilized instantaneous characteristic features (ICF) of the thigh during SN as a key factor for classifying stair ascent, descent, walking, sitting, and standing. Their approach relied on a state machine to detect transitions between these activities. Similarly, Bartlett and Goldfarb [42] employed a phase-space-based coordinate system derived from thigh motion, providing a feature set applicable to common pattern recognition methods for gait and stair activities. This approach functioned effectively using only a 6-axis IMU. Chinimilli et al. [43] demonstrated that using a single IMU on the thigh to measure angular displacement and velocity enabled classifiers to accurately detect uphill/downhill walking and stair ascent/descent. Young and Hargrove [44] took a different approach by applying LDA classifiers with data from 13 IMUs to develop a user-independent recognition system. Their model successfully detected transitions between walking and stair climbing for transfemoral amputees.

The main challenges in HAR system research include the need for large datasets to train models, difficulties in real-time implementation, and the inclusion of older adults in the models. Most existing models have been developed and tested using data from healthy young adults, which limits their applicability to older populations. Age-related physiological changes, such as reduced mobility, non-alternating leg (NAL) patterns during stairs negotiation (SN), and slower reaction times, significantly influence the movement patterns of older adults.

In this study, we propose a lightweight human activity recognition (HAR) method for real-time implementation on smartphones, using minimal body-worn IMUs and biomechanics-based classifiers. As a physics-based framework, our model relies on biomechanical features, maximum and minimum angle values of the thigh and foot, which are physically interpretable and representative of key gait events. Rather than introducing a complex new neural network architecture, our contribution lies in the development of a computationally efficient and practically deployable classifier that can be trained with a small dataset, reducing the dependency on large training samples, while maintaining high accuracy. The offline model was trained using heuristic ML algorithms, including SVM, KNN, NB, and LDA, and it was implemented in real-time by developing a KNN classifier, for their low computational cost and ease of implementation on resource-constrained devices. The model uses two IMUs placed on a single leg (thigh and foot) to extract biomechanical features in real-time. To support real-time applications, an adaptive segmentation strategy for toe-off detection in various activities was also implemented. The statistical results show how biomechanical features obtained from young adults could be used to train a model that remained effective for older adults. So, the system can be applicable to older adults and is also capable of detecting non-alternating leg (NAL) stair negotiation (SN), as a prevalent mobility issue in older adults, where they rely on one leg during stair negotiation. Furthermore, deploying the model on a smartphone can promote its practical application in home-based health monitoring systems, particularly for older adults with mobility limitations or NAL patterns during SN (NAL-SN pattern). The contributions of this paper are listed below:

- Development of a lightweight HAR model optimized for real-time application deployed on a smartphone by using minimal but meaningful biomechanical features.
- Utilization of lower-limb biomechanical features for training the model with accurate activity recognition using ML algorithms and minimizing computational cost.
- Training the model on young adults and testing it on young and older adults to assess its generalizability.

- Implementation of the NAL-SN pattern by training the model with the NAL-SN patterns of young adults and deploying it for older adults with this condition.

The lack of models for older adults impedes deploying HAR systems for health monitoring applications. A HAR system that accounts for the movement limitations of older adults can be used in wearable devices for gait training [45], [46], [47] as well as for daily activity monitoring in the users' natural and functional settings such as the home. This work bridges the gap between advanced HAR research and practical applications for older adults, offering a robust data-efficient solution for real-time implementation.

II. METHOD

A. PARTICIPANTS

A total of 25 participants were recruited for the study, divided into young and older adult groups. The inclusion criteria for recruiting participants were the ability to walk (W) and stair negotiation (SN) independently for about 15 minutes, while using handrails for assistance was permitted. Exclusion criteria included diagnosed neuromuscular diseases (e.g., Parkinson's disease, stroke, multiple sclerosis, etc.), cognitive impairment, or cardiopulmonary disease. Participants were further divided into subgroups for training and testing the model described below:

- Group 1 (young normal training group): 10 young adults (5 females, age: 24.4 ± 3.6 years) were recruited to collect data to train the system with regular W and SN patterns.
- Group 2 (young normal testing group): 5 additional young adults (3 females, age: 31.2 ± 5.9 years), different from participants in Group 1, were recruited for testing the model trained by Group 1. These participants followed regular W and SN patterns.
- Group 3 (young non-alternating leg (NAL) training group): The same participants from Group 1 (i.e., young participants for model training) were recruited again to expand model training by including the NAL-SN as observed in older adults. The participants were instructed to ascend and descend stairs using only one of their legs as the leading leg as opposed to the normal alternating pattern, in which both legs take turns to lead.
- Group 4 (young non-alternating leg (NAL) testing group): The same participants from Group 2 (i.e., young participants for model testing) were instructed to perform SN with the NAL pattern to test the extended model trained by Group 3's data.

After completing the training and testing phases with young adults, older adult participants were recruited in the following groups to test the robustness and applicability of the models across different age groups and NAL-SN patterns.

- Group 5 (older normal testing group): 6 older adults (3 females, age: 75.8 ± 6.7 years) performed regular walking and SN.
- Group 6 (older non-alternating leg (NAL) testing group): 4 older adults (2 females, age: 72.7 ± 4.3 years) performed NAL-SN and regular W.

In total, 25 participants were involved in the study: 15 young adults (10 for model training and 5 for model testing) and 10 older adults for model testing. The same young participants, either for training or testing, contributed to both normal and NAL trials. The study was approved by the University of Maine Institutional Review Board (IRB protocol number 2019-0-15). All participants provided written informed consent before participation.

B. FEATURE SELECTION

The primary aim of this study was to develop a model capable of classifying and detecting functional mobility tasks with minimal data and computational cost and limited available data, making it applicable to individuals of different ages. This study focused on five key activities: standing (ST), sitting (SI), walking (W), and stair ascending (SA)/descending (SD). Data were collected using IMUs to enable real-time classification. Previous studies, such as the work by Cheng et al. [41], utilized a single IMU on the thigh combined with a force-sensitive resistor (FSR) to detect heel-strikes for window segmentation. Then, the maximum thigh angle was identified as a critical feature for detecting transitions between activities. Inspired by this approach, our study utilized two IMUs on one leg: one placed on the front side of the thigh and the other on the back of the shoe as shown in Fig. 1 (a).

To extract features for classification, four biomechanical features shown in Fig. 1(b) were selected: max thigh angle (θ_T^{Max}), min thigh angle (θ_T^{Min}), max foot angle (θ_F^{Max}), and min foot angle (θ_F^{Min}) from the thigh and the foot IMUs during each activity cycle. Fig. 2 demonstrates the biomechanical features during standing (ST), walking (W), stair ascending/descending (SA/SD), and sitting (SI). These features were selected based on both their biomechanical relevance and statistical separability. The maximum thigh angle captures peak hip flexion, which significantly increases during stair ascent, while the minimum thigh angle reflects postural depth, especially relevant during stair descent. The minimum foot angle corresponds to the toe-off event and often changes sign depending on the activity, and the maximum foot angle aligns with heel-strike. Moreover, our statistical analyses, presented in the results section, showed that thigh angle features differed significantly across activities and foot angles during walking and stair negotiation. These features had low overlap, supporting their discriminative power for use in the model. They allowed the system to remain lightweight, minimizing computational cost while preserving the accuracy of the model.

C. SEGMENTATION

To process the streamed data from the IMUs, windowing techniques are essential for segmenting the data into

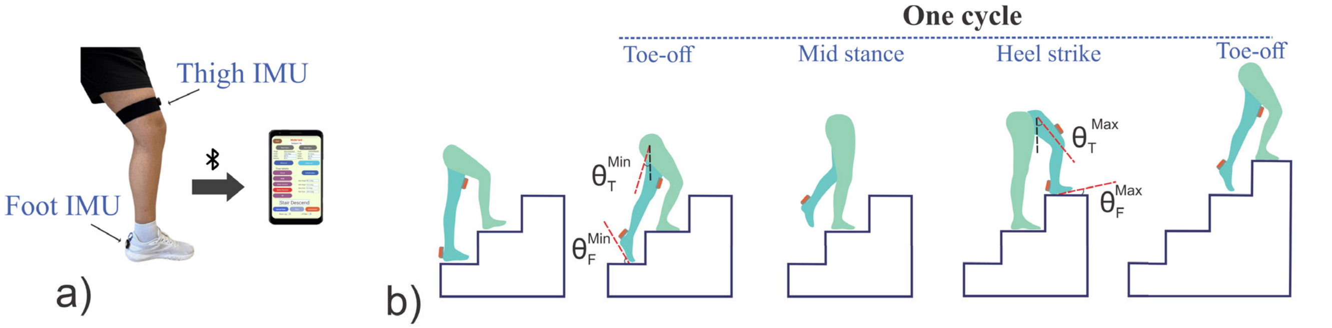

FIGURE 1. **(a) Placement of thigh and foot IMU on a participant showing the connection of the IMUs to the developed Android system application with Bluetooth and (b) the complete cycle of stairs ascending (SA) from the toe-off moment as the criteria for segmentation for the next toe-off with showing the location of the IMUs.**

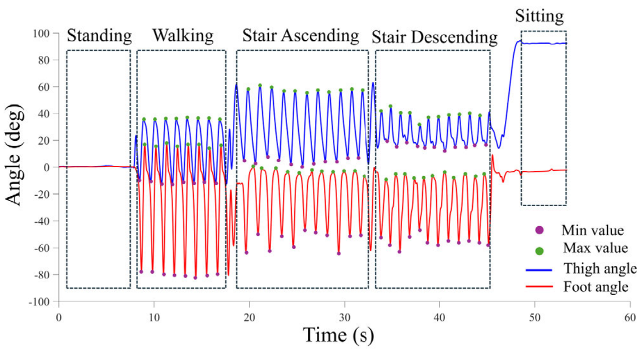

FIGURE 2. **The thigh and foot angles during the standing (ST), sitting (SI), walking (W), and stair ascending/descending (SA/SD). For a clearer demonstration, a 4th-order Butterworth low-pass filter with a 6 Hz cut-off frequency was used [48].**

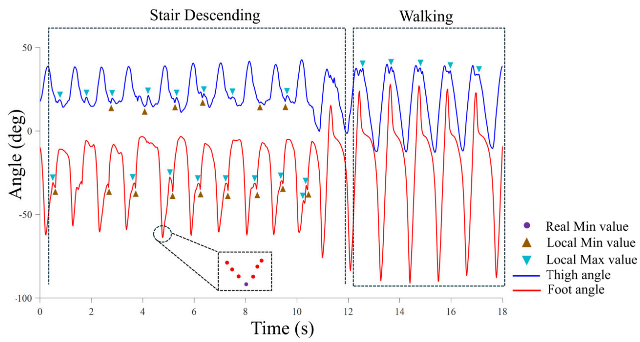

FIGURE 3. **Fluctuations and the presence of local peaks in thigh and foot angles, showing the real minimum foot value as the criteria for adaptive segmentation.**

meaningful intervals for analysis. These techniques can be categorized as either fixed or adaptive, depending on the requirements of the model. Fixed windowing segments the data based on a predefined time length, streaming the collected data with a specified overlap. The fixed window size can lead to inaccuracies when the activity has different duration times as well as transition moments of the activities [49], [50]. Furthermore, a significant limitation of fixed windowing is its time latency, as the processing of captured data can only begin once the window reaches its full length. Although fixed windowing is commonly used in recent studies, particularly in models employing CNNs for real-time activity detection, it is less suitable for applications requiring the fastest possible processing [51]. Therefore, adaptive windowing, which allows for faster segmentation by dynamically closing windows based on specific criteria, was selected for this study.

The efficacy of adaptive windowing depends on the appropriate segmentation criterion. In level walking experiments, heel-strike and toe-off are important events for evaluation of the movement [52]. The heel-strike moment is typically used as the segmentation criterion. However, our analysis revealed that during SN, particularly SA, the heel-strike moments were less distinct and harder to detect due to fluctuations and the presence of local peaks in both thigh and foot IMU readings, as shown in Fig. 3. While some studies, such as Chinimilli et al. [43], have used the maximum thigh angle as the segmentation criterion; however, our study found that the toe-off moment, corresponding to the minimum foot angle or (i.e., the maximum foot dorsiflexion) provided a more reliable and consistent basis for segmentation. This approach was particularly effective in detecting W and SN activities, ensuring accurate and timely segmentation even under challenging conditions. The toe-off was considered both the criterion for segmentation and a feature for the classification.

Fig. 3 demonstrates the thigh angle (TA) and foot angle (FA) during W and SD, highlighting the fluctuations inherent in these movements. Due to the nature of these activities, numerous local peaks exist for both the maximum and minimum values, making it challenging to identify the true peaks. For example, during SA, the pattern of the heel-strike, defined by the maximum FA, differs significantly from normal W, making heel-strike unsuitable as a criterion for segmentation. Conversely, toe-off, defined by the minimum FA, exhibits local variations and fluctuations, but specific criteria can help distinguish the actual toe-off from these local peaks. These criteria are informed by experimental data and previous studies on the biomechanics of walking and stair climbing:

1) The first criterion ensures that consecutive toe-off events are separated by a minimum time threshold set at

0.4 s in this study. This value accommodates the typical movement cycle of both young and older adults who can W or SN independently.

2) The second criterion considers the biomechanics of toe-off, requiring the angle at this event to exceed a specific threshold. In this study, the threshold was set at $-30°$, ensuring the detected peak aligns with the expected range for toe-off in walking and stair climbing. These criteria collectively improve segmentation accuracy by minimizing the detection of local fluctuations.

The process for selecting the threshold values used in the segmentation criteria is detailed in Appendix A, including the empirical analysis and statistical validation supporting their selection. These adaptive segmentation criteria were only used for W and SN; given that there are no toe-off moments during SI and ST, a sliding window was used as a technique for segmentation. Because SI and ST are static poses of the body, the disadvantage of using sliding windows did not impact the results. The window length was 0.5 s [53]. In each window, while standing and sitting, the max and min values should be almost the same for the thigh and foot.

D. DATA COLLECTION

Using the adaptive segmentation technique based on toe-off for W and SN as well as fixed windowing for ST and SI, the maximum and minimum values of the foot and thigh angles (θ_T^{Max}, θ_T^{Mmin}, θ_F^{Max}, θ_F^{Min}) were extracted for each segmented window. These features capture the essential biomechanical patterns of the activities while minimizing computational complexity. The features during a cycle of SN are demonstrated in Fig. 1 (b), where the IMUs can be on the left or right leg. As visualized in a three-dimensional space in Fig. 4, the resulting point clouds displayed the relationship between the maximum and minimum values of TA and the minimum value of FA across different classes of activities. Each activity formed distinct clusters in this space with boundaries that were separable. This distribution highlights the discriminative power of the selected features, confirming their suitability for classification. The distinct separation of activities in the feature space underscores the robustness of the approach and its potential for accurate activity recognition across a range of daily tasks. The visualization proves the feature selection process, demonstrating how these biomechanical metrics inherently differentiate the activities under study.

E. CLASSIFIERS

Due to the simplicity of the one-dimensional feature space derived from four values in each segmented window of IMU stream data, heuristic feature-based machine learning algorithms were utilized. For offline training, KNN, LDA, SVM, and NB classifiers were implemented. The training process was conducted offline using Google Colab and the Scikit-learn library. After evaluating the accuracy of each model, the algorithm with the best performance was

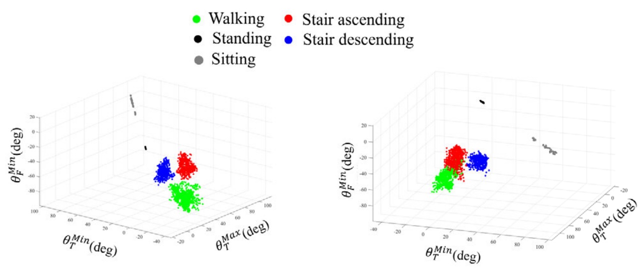

FIGURE 4. Two views of three-dimensional cloud for max and min of thigh angles (TA) as well as min foot angle (FA), [θ_T^{Max}, θ_T^{Min}, θ_F^{Max}, θ_F^{Min}]. These features represent key gait characteristics that were extracted from IMUs and are used to train the model to classify the activities.

selected for real-time deployment. The real-time model was implemented on an Android system using a smartphone shown in Fig.1(a). Deployment on the Android Studio platform required manual integration of the chosen classifier by defining its logic in Java. This approach ensured the model could function efficiently in a real-time mobile environment.

F. RECOGNITION MODEL LOGIC

The model's logic is outlined in Algorithm I. It includes two windowing techniques: an adaptive window for real-time data streaming from the foot and thigh, and a fixed-length smaller window to detect the exact toe-off events. The adaptive window started storing the data when a toe-off was detected and closed the window at the next toe-off, meanwhile the collected data was analyzed to extract the maximum and minimum values for the classification (see lines 6-10 in I). The fixed-length window of seven samples (captured at 60 Hz covering a duration of approximately 116 ms) was used to detect toe-off within the adaptive window. As shown in Fig. 3, the criterion for toe-off detection required that the middle sample in this window to be the minimum and fall below a predefined threshold, as described in Section II-E. The index of IMU data served as the timing reference. To ensure sufficient separation between consecutive toe-off events, the detected index needed to meet a minimum threshold distance from the previous one (see Section II-C). When a toe-off was detected, the middle array's sample for the foot data was marked as the new toe-off index. Otherwise, if the detected value was a local peak or regular data point, the foot and thigh angles were stored in the adaptive window for segmentation (see lines 1-5 in Algorithm I).

G. NON-ALTERNATING LEG (NAL) MODEL

The SA and SD are activities that often pose challenges for community-dwelling older adults. Over time, they may struggle to perform these tasks as smoothly as healthy young individuals. When older adults encounter difficulties with stair climbing, they may rely on handrails for support or adopt an alternative strategy to maintain balance, such as avoiding alternating their legs during climbing. Instead, they may use a single leg as the "lead leg" to ascend or descend stairs [54], [55].

Algorithm I Recognition Model Logic

Input: θ_T^{new} and θ_F^{new} as the current sample of thigh and foot angles
Output: Recognized activity
Initialize:

- Streaming IMUs data at 60 Hz
- Creation of seven variables to find toe-off: $\left[\theta_F^1 \; \dots \; \theta_F^7\right]$
- Creation of arrays for windows of samples: $\bar{\mathbf{W}}_T$, $\bar{\mathbf{W}}_F$
- $Ind(\theta_F^{toe-off}) = 0$

Streaming data for thigh and foot: θ_T^{new}, θ_F^{new}

$\theta_F^{i-1} \leftarrow \theta_F^i$ for $i = 2$ to 7 and $\theta_F^7 \leftarrow \theta_F^{new}$

if $\theta_F^4 < \theta_F^i$, **and** $\theta_F^4 < AngleThreshold$,
and $|Ind(\theta_F^4) - Ind(\theta_F^{toe-off})| > TimeSeparationThresholdIndices$ **then**

  \# θ_F^4 is the toe-off moment for closing the windows

  $Ind(\theta_F^{toe-off}) = Ind(\theta_F^4)$

  $\left[\theta_T^{\text{Max}} \; \theta_T^{\text{Min}} \; \theta_F^{\text{Max}} \; \theta_F^{\text{Min}}\right] \leftarrow$ Find max and min values of W_T and W_F

  Recognized activity $\leftarrow$ Classifier $(\theta_T^{\text{Max}}, \theta_T^{\text{Min}}, \theta_F^{\text{Max}}, \theta_F^{\text{Min}})$

  Clear $\bar{\mathbf{W}}_T$ and $\bar{\mathbf{W}}_F$

else

  $\bar{\mathbf{W}}_F \xleftarrow{\text{append}} \theta_F^{new}$ and $\bar{\mathbf{W}}_T \xleftarrow{\text{append}} \theta_T^{new}$

end if

Return Recognized activity

Given that this study's objective was to develop a robust activity recognition model, it was essential to ensure the system could accommodate older adults with normal W and SN patterns as well as abnormal SN patterns. Therefore, in addition to the primary activities (i.e., standing, sitting, stair ascending, and stair descending) two additional activities were incorporated to enhance the model's robustness: non-alternating legs stair ascending (NAL-SA) and descending (NAL-SD), where one leg consistently led.

With this expanded scope, an important question was: on which leg should the IMUs be placed? Should they be positioned on the lead leg, responsible for most of the movement, or on the trailing leg? Answering this question necessitated revisiting the segmentation criteria for the IMU data, as segmentation is a critical factor for effective data analysis and accurate activity detection. By thoroughly examining the segmentation process, we aimed to determine the IMU placement for reliable classification across different SN patterns. Fig. 5 shows an example of NAL-SA pattern where the left leg is the leading one. However, the IMUs are located on the right leg as the trailing one.

To evaluate the placement of the IMUs and the changes in thigh and foot angles during NAL pattern, the participants in group 3 were first instructed to avoid alternating their legs during stair negotiation, with the IMU placed on the leading leg. The results of this setup are presented in Figs. 6(a), (c). In the second trial, the IMUs were placed on the trailing leg, with the results shown in Figs. 6(b), (d). The undesired local peak values of the foot angle are more noticeable when the IMUs were placed on the leading leg (Figs. 6(a), (c)). While offline analysis can effectively filter out these

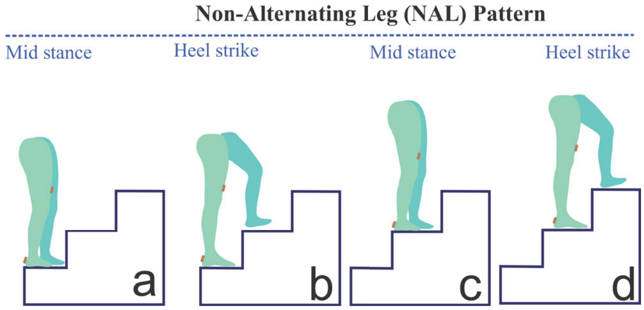

FIGURE 5. Non-alternating leg (NAL) pattern for stairs negotiation (SN) showing the left leg is the leading side and the IMUs are located on the right leg as the trailing one.

local peaks for segmentation, the real-time detection of the toe-off, as the minimum foot angle, was less accurate with IMU on the leading leg. The trailing leg's patterns during NAL-SN are similar to the patterns during normal SN (Figs. 6(b), (d)). Unlike the leading leg, which deviated from the normal movement patterns to establish a new stable climbing strategy, the trailing leg maintained movement characteristics similar to normal climbing. Fig. 7 illustrates the cloud of points representing the features when the IMUs were placed on the trailing leg during NAL-SN. Overall, for non-alternating leg stair climbing, the IMUs should be placed on the trailing leg, given this reduces the inaccuracies in real-time segmentation.

Compared to Fig. 4, there is a greater overlap between clouds for the features, particularly normal SA and NAL-SD patterns. However, the clusters remain sufficiently distinct to be separable by a well-fitted classifier model. The observed increased overlap between NAL and normal feature clusters (compared to Fig. 4) is expected for a lower classification accuracy for the NAL patterns model compared to the normal patterns model, particularly for NAL-SD detection. Nonetheless, the system was still expected to differentiate between normal and NAL patterns while identifying the movement type as either SA or SD.

H. DEPLOYMENT OF THE MODEL

To design the system and collect data, the Movella (Xsens Technologies B.V., Enschede, The Netherlands) IMU SDK was used to program an Android-based environment on a smartphone. A Google Pixel 6a (Google LLC, Mountain View, CA, USA) was chosen as the device for development. The process started by creating software to collect raw IMU data. Once collected, the raw data were processed in MATLAB (MathWorks Inc., USA, 2024) to segment windows, and the resulting data were prepared for classifier training. The classifiers were trained using Python in Google Colab (Google LLC, Mountain View, CA, USA), and the best model was selected. The model's coefficients were extracted and implemented into a real-time system on the smartphone. For the second phase of smartphone application development, the classifier was coded in Java, incorporating all the criteria necessary to detect peak values and identify toe-off moments.

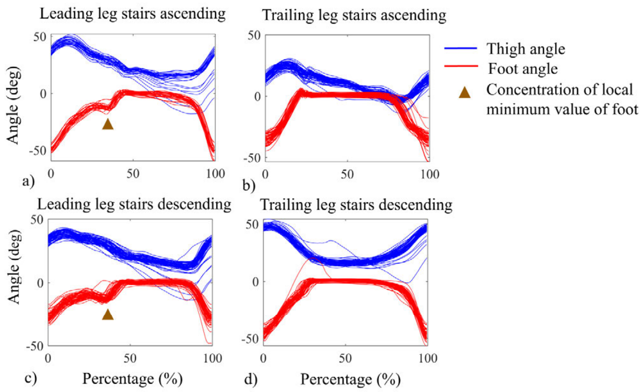

FIGURE 6. **Variations in foot and thigh angles during non-alternating leg stair ascending (NAL-SA) and descending (NAL-SD) within the offline segmented window, cycle-based on toe-off moments, indicate a higher occurrence of local peaks in the lead leg-mounted IMU. This suggests that mounting the IMU on the lagging leg is a better choice, as it enhances real-time segmentation accuracy.**

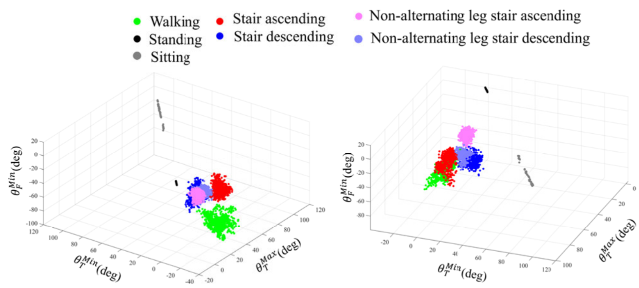

FIGURE 7. **Three-dimensional cloud for max and min of thigh angles (TA) as well as min foot angle (FA), $[\theta_T^{Max}, \theta_T^{Mmin}, \theta_F^{Max}, \theta_F^{Min}]$ for all activities with also non-alternating stairs negotiation (NAL-SN). Greater overlap is observed among the activity clusters compared to the normal-only dataset, which is expected to contribute to the reduced classification accuracy in the NAL-SN condition.**

These features were used to segment the streamed IMU data in real-time. The application allowed real-time testing with participants, displaying activity detection results during experiments. Upon completing an experiment, the application generated a confusion matrix to report the system's accuracy for each participant. An example of using the real-time model with a participant is depicted in Fig. 8.

The computational cost and processing delay are critical for real-time applications. The manual implementation of the classifier in Java on the Android system ensured efficient performance. Once a segmented window was created and the four features (θ_T^{Max}, θ_T^{Mmin}, θ_F^{Max}) were extracted, the classifier was called, resulting in a processing delay of just 2 ms. Detecting toe-off, a key factor for the classifier, required 50 ms due to the IMU's 60 Hz sampling frequency. Therefore, the total processing time, including data segmentation and activity classification, was approximately 52 ms. This means that when a participant transitions from walking to stair climbing, the system identified and displayed the new activity within 52 ms. This processing time is acceptable for real-time activity monitoring systems given the reported values of 80 ms [43] and 240 ms [56] in the literature. This quick response demonstrates the system's suitability for real-time monitoring of movement activities.

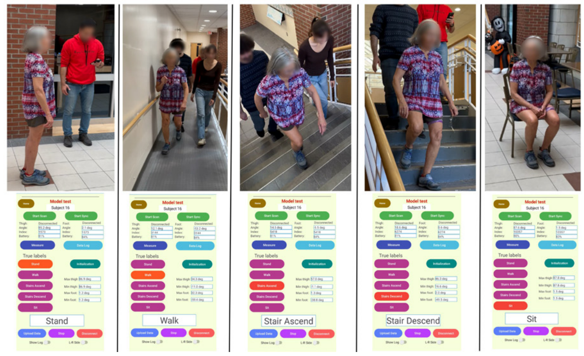

FIGURE 8. **An example of using the developed app for data collection and a participant while the real-time model could recognize the activity.**

Regarding the error of the IMUs, the Movella DOT internally fuses accelerometer, gyroscope, and magnetometer signals using a Kalman filter. It provides orientation accuracy of 0.5° RMS for inclination and 1.0° RMS for heading under static conditions, and 1.0°/2.0° RMS for inclination and heading, respectively, under dynamic conditions. Signal quality was further evaluated using Signal-to-Noise Ratio (SNR) (see Appendix B), in which SNR values were consistently above 25 dB across all participants and activities, indicating high-quality signals [57]."

III. EXPERIMENTAL DESIGN

A. LOCATION DESCRIPTION

The experiments were carried out in two indoor environments on the University of Maine campus. These locations were chosen because they closely resemble everyday home- and community-based settings that people encounter, making them ideal for simulating real-life activities. The selected environments facilitated the targeted activities, including stair climbing, sitting, level walking, and ramp walking, to ensure the model's robustness in detecting walking modes. Both the training and testing phases of the study were conducted within these locations.

The locations' information is presented in Table 1. Location 1 path was a closed-loop route, beginning with level-ground walking from a designated starting point. Participants walked approximately 3 m on level ground before reaching a staircase. The staircase consisted of 28 steps, organized as two sets of 14 steps, with a landing in between. Each step measured 31 cm in width and 17 cm in height. Participants ascended to the second floor, walked about 22.5 m on level ground, and then descended the same staircase back to the first floor. After descending, participants walked another 47 m back to the starting point. Additionally, a lobby area with seats was included for the sitting experiment.

Location 2 included a closed-loop route with a ramp segment. Walking up and down the ramp was included to

TABLE 1. Information and dimensions of the experiment locations.

Item	Location 1	Location 2
Walking distance	70 m	42 m
Stairs number (each ascend/descend)	28	22
Stairs size	H: 17 cm × D: 31 cm	H: 17 cm × D: 31 cm
Ramp incline	-	4°
Ramp distance	-	15 m

classify them as a walking activity and differentiate them from other activities such as stair negotiation. Participants started with level-ground walking and then transitioned to a ramp segment. The ramp was approximately 15 m long with a 4° incline. Following the ramp, participants ascended a staircase consisting of 22 steps, arranged as two sets of 11 steps with a turning spot in between. The steps in this staircase were slightly different than the ones in location 1, measuring 31 cm in width and 17 cm in height. After ascending, participants immediately turned back, descended the stairs, and continued walking on level ground to return to the starting point. This location also included seating to facilitate sitting activities.

These two environments were chosen to provide a diverse and realistic condition for the experiment. The first location offered a typical staircase-focused setup, while the second location introduced a ramp segment to evaluate the system's ability to distinguish ramp walking from other activities. Both locations enabled adequate data collection for training and testing the activity recognition system in a controlled real-world setting.

B. OFFLINE EXPERIMENT

The offline experiments were considered as the data collection for training the model and evaluating the classifier in the offline mode with the collected data. Groups 1 and 3, consisting of young adults, participated in experiments to collect biomechanical data and train the model. Both groups completed trials in both locations. In location 1, group 1 was instructed to complete four rounds of a predefined activity loop. This loop included standing still for a few seconds to initialize the IMU values, W, SN, and finally sitting on a standard chair for about 60 s. A similar procedure was followed in location 2, with the key difference of including walking on a ramp to collect data for walking on inclined surfaces. Group 1 repeated the activities for four rounds in this environment.

The main difference for group 3 was during the SN phase. Participants were asked to use the NAL patterns, relying on a single leg for both SA and SD. They were first asked to identify their leading and trailing legs and were then instructed to maintain it throughout the activity. The IMUs were placed on the trailing leg according to the criteria outlined in section II-G. Participants could use handrails for support if needed and could take a break at any point during the experiments to ensure their comfort and safety. For both groups, participants were asked to complete the four activity loops with varying speeds. During the first two rounds, they maintained a normal W and SN pace, while for the final two rounds, they increased their speed. This approach could help collect data across different activity speeds, enhancing the robustness and adaptability of the model.

During the training sessions, data were collected through a custom application with buttons corresponding to each activity to label the activities for training the model. An operator, maintaining a safe distance to avoid distracting the participant, used these buttons to annotate the IMU data stream in real-time. The operator pressed the corresponding button at the beginning of each activity and released it at the end, signaling the transition to the next activity. While there were no time limits for each activity, efforts were made to collect sufficient data to ensure a complete dataset for training. Each button press appended specific indices to the streaming IMU data, which were later saved as CSV files for offline processing and experimental validation.

C. REAL-TIME EXPERIMENT

The real-time experiments were designed to test the trained model and evaluate its accuracy in detecting activities. Groups 2 and 4, consisting of young adults, participated in this test and completed the experiments in both locations. Group 2 was asked to perform the activities in a loop four times in each location, following the same procedures as described in the previous section. Similarly, Group 4 completed the same loops but with a focus on NAL patterns. To test the model's performance across different activity speeds, the first two loops were conducted at a normal speed, and the remaining two were performed at a faster speed.

For Groups 5 and 6, consisting of older adults, additional accommodations were made to prioritize their safety and comfort. To ensure the participants could complete SA and SD independently, the Functional Gait Assessment (FGA) [58] was completed. The FGA consists of 10 test items, each scored from 0 (severe impairment) to 3 (normal ambulation), for a total maximum score of 30 [59]. The scores reflect a range of mobility levels and were used to invite participants who could negotiate stairs independently.

All tests for groups 5 and 6 were conducted in location 2. To minimize fatigue, participants could stop the session at any time if they felt tired or unable to continue. Ideally, they were asked to complete three loops of the activity sequence, but if they felt capable, they were encouraged to do additional rounds to provide more data for the study. Group 5 performed the activities, including level W, ramp W, and SN, at a normal speed for the first two loops and a faster speed for the final loop. Group 6 followed a similar procedure but with the additional step of selecting a preferred leading leg for SN. IMUs were placed on their trailing leg. Handrails were made available for their safety, and two team members accompanied them during the activities: one walked ahead, one followed closely behind, and a third operator managed the smartphone application to run the test.

TABLE 2. Group of participants' information and physical characteristics.

No.	Group Name	Age Group	No.	Age	Height (cm)	Weight (kg)	FGA Score
Group 1	Young normal training	Young adults	10 (5 F)	24.4 ± 3.6	178.5 ± 7.6	75.9 ± 16.8	-
Group 2	Young normal testing	Young adults	5 (3 F)	31.2 ± 5.9	176.0 ± 13.0	78.2 ± 12.7	-
Group 3	Young non-alternating training	Young adults	10 (5 F)	24.4 ± 3.6	178.5 ± 7.6	75.9 ± 16.8	-
Group 4	Young non-alternating testing	Young adults	5 (3 F)	31.2 ± 5.9	176.0 ± 13.0	78.2 ± 12.7	-
Group 5	Older normal testing	Older adults (>65)	6 (3 F)	75.8 ± 6.7	172.7 ± 13.0	69.7 ± 8.2	24.6 ± 6.0
Group 6	Older non-alternating testing	Older adults (>65)	4 (2 F)	72.7 ± 4.3	170.5 ± 9.5	80.0 ± 6.2	22 ± 3.5

To evaluate the accuracy, the developed application detected the predicted activity in real-time during the test. The operator manually labeled each activity using the smartphone application as a reference, similar to the offline experiment. The program compared the predicted label with the true label, counting a match as correct and a mismatch as incorrect. Regarding the prediction delay, as noted in section II-H, the application detected the activity with a 52 ms delay after a transition to a new activity, while the operator was instructed to promptly label the new activity as soon as it was observed. The application completed the comparison of the results, and the final results of that participant were reported after completing the experiment.

IV. RESULTS

A. PARTICIPANTS

The participants' information, including the ratio of sex, age, height, and body mass for each group explained in section II-A are presented in Table 2. The FGA scores for Group 5, consisting of six participants, were 28, 30, 26, 26, 13, and 25. All participants in this group were able to SN with leg alternation. However, the FGA scores for Group 6, comprising four participants, were 27, 19, 20, and 22. Participants in this group were instructed to follow the NAL pattern for SN.

B. BIOMECHANICAL FEATURES

The mean and standard deviation of the features including θ_T^{Max}, θ_T^{Mmin}, θ_F^{Max}, and θ_F^{Min} in each segment for all activities across the groups are presented in Table 3. The classification model's performance in offline and real-time modes was based on these features, where the differences between the activities are apparent from the values.

C. STATISTICAL ANALYSIS

The goal of statistical analysis was to determine how the biomechanical features, as the dependent variables, changed across different activities of W, SA, and SD and for the two age groups (the independent variables). Mixed-effect repeated Measures ANOVA (Analysis of Variance) with a significance level of $\alpha = 0.05$ was performed using SPSS v29 (SPSS Inc., Chicago, IL, USA). The within-subjects factor was the type of activity (i.e., W, SA, and SD), the between-subjects factor was age group (i.e., young adults in group 1 and 2 and older adults in groups 5 and 6), and the interaction between the two factors (i.e., activity × age) was also considered. For the statistical analysis, we only used the normal pattern of SN.

TABLE 3. The biomechanical features for each group reported as mean and standard deviation.

No.	Activity	Max. thigh (deg)	Min. thigh (deg)	Max. foot (deg)	Min. foot (deg)
Group 1	Walk	34.44 ± 5.47	-14.35 ± 3.80	30.35 ± 3.81	-75.83 ± 8.49
	Stairs ascend	52.65 ± 5.34	-2.49 ± 3.37	-2.24 ± 5.00	-47.18 ± 7.07
	Stairs descend	39.70 ± 5.37	12.11 ± 3.50	-2.61 ± 2.47	-52.83 ± 4.00
Group 2	Walk	36.42 ± 6.57	-16.14 ± 5.88	33.90 ± 6.33	-74.23 ± 4.53
	Stairs ascend	59.30 ± 9.36	0.64 ± 9.90	1.75 ± 3.07	-45.09 ± 6.75
	Stairs descend	44.30 ± 11.42	15.45 ± 8.45	-1.60 ± 3.01	-49.37 ± 5.22
Group 3	Walk	36.31 ± 7.42	-15.89 ± 6.34	33.15 ± 7.53	-72.43 ± 5.41
	Stairs ascend	60.16 ± 2.34	-1.62 ± 4.03	7.06 ± 3.99	-43.12 ± 5.09
	NAL Stairs ascend	27.71 ± 10.36	-0.23 ± 3.30	4.28 ± 2.22	-34.18 ± 10.05
	Stairs descend	42.65 ± 3.57	9.56 ± 5.03	-0.11 ± 1.48	-49.52 ± 2.14
	NAL Stairs descend	42.87 ± 3.95	6.22 ± 6.64	1.10 ± 1.65	-42.42 ± 3.13
Group 4	Walk	35.18 ± 7.24	-15.90 ± 5.97	31.75 ± 8.06	-71.20 ± 5.18
	Stairs ascend	59.44 ± 1.99	-1.13 ± 4.10	6.50 ± 3.42	-43.06 ± 7.57
	NAL Stairs ascend	27.85 ± 8.68	-1.18 ± 4.08	5.69 ± 2.66	-33.35 ± 2.57
	Stairs descend	43.97 ± 2.78	10.74 ± 5.53	0.18 ± 1.81	-48.25 ± 2.51
	NAL Stairs descend	41.64 ± 9.38	5.31 ± 5.96	-0.26 ± 1.42	-41.94 ± 6.52
Group 5	Walk	31.68 ± 6.88	-13.34 ± 3.69	25.87 ± 5.93	-61.20 ± 8.92
	Stairs ascend	56.32 ± 5.30	-3.20 ± 2.40	0.73 ± 2.67	-50.31 ± 5.96
	Stairs descend	41.24 ± 9.03	9.95 ± 5.63	0.03 ± 1.82	-51.76 ± 8.62
Group 6	Walk	31.64 ± 4.61	-13.03 ± 1.45	26.14 ± 0.68	-63.50 ± 3.54
	Stairs ascend	60.67 ± 2.57	-1.97 ± 11.42	6.67 ± 0.30	-44.73 ± 16.24
	NAL Stairs ascend	28.79 ± 3.47	-2.68 ± 8.09	6.33 ± 3.25	-32.27 ± 5.27
	Stairs descend	42.10 ± -0.10	11.86 ± 14.55	0.52 ± -4.42	-49.03 ± -1.71
	NAL Stairs descend	43.04 ± 18.30	5.87 ± 8.15	0.46 ± 6.83	-40.99 ± 10.20

Fig. 9 shows the bar plots of the dependent variables of θ_T^{Max}, θ_T^{Min}, θ_F^{Max}, and θ_F^{Min}. Significant differences were found for θ_T^{Max} ($F(2, 23) = 278.78$, $p < 0.001$, $\eta^2 = 0.924$), θ_T^{Min} ($F(2, 23) = 322.65$, $p < 0.001$, $\eta^2 = 0.933$), θ_F^{Max} ($F(2, 23) = 520.87$, $p < 0.001$, $\eta^2 = 0.980$), and θ_F^{Min} ($F(2, 23) = 163.09$, $p < 0.001$, $\eta^2 = 0.921$) across the three activities, W, SA, and SD. Post-hoc analysis revealed that for all the dependent variables (θ_T^{Max}, θ_T^{Min}, θ_F^{Max}, θ_F^{Min}), there were significant differences between the W and SA as well as the W and SD ($p < 0.001$). For θ_T^{Max}, θ_T^{Min} ($p < 0.001$), and θ_F^{Min} ($p = 0.004$), there were also significant differences between the SA and SD; however, there was no significant difference between the SA and SD for θ_F^{Max}.

The main effect of age (young vs. older adults) was not statistically significant, but this does not imply that age had no influence. Significant interaction effects between age and activity were observed. Differences between older and young adults were found in θ_F^{Max} and θ_F^{Min} in the W activity ($p = 0.015$ and $p<0.001$) as well as for θ_F^{Max} in the SD activity ($p = 0.016$).

D. OFFLINE EXPERIMENT

The offline experiment was designed to collect data and train the classifiers. The total number of sample data points

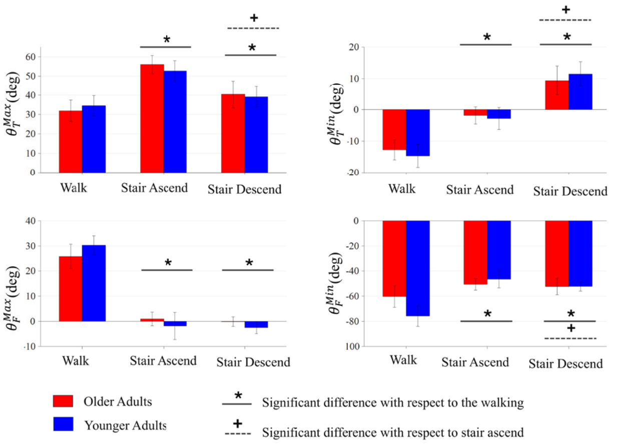

FIGURE 9. The bar plots of the biomechanical features across three different activities and for the young- and older-adult participants, with error bars showing standard deviations.

TABLE 4. Sample data as the segmented window for each activity.

Normal Pattern	Stand	Walk	Stairs Ascend	Stairs Descend	Sit
Sample Data	588	1891	1246	1210	682
NAL Pattern	Stairs Ascend	NAL Stairs Ascend	Stairs Descend	NAL Stairs Descend	
Sample Data	732	702	751	768	

TABLE 5. Results of accuracies of the classifiers as the offline testing of the model.

Normal Pattern				
Type of Classifiers	**SVM**	**LDA**	**NB**	**KNN**
Thigh features	91.43%	89.32%	91.28%	92.03%
Thigh and foot features	99.90%	99.79%	100%	100%
NAL Pattern				
Type of Classifiers	**SVM**	**LDA**	**NB**	**KNN**
Thigh features	85.46%	86.70%	87.18%	86.62%
Thigh and foot features	97.53%	96.40%	96.21%	96.64%

collected during the experiments is summarized in Table 4. Each sample corresponds to a segmented window of activity. For dynamic activities like SN and W, segmentation was performed based on toe-off moments, which served as the criteria for defining windows. The static activity examples like standing and sitting, a fixed window size of 0.5 s was applied for segmentation.

Four classifiers were chosen for training and testing with the offline dataset: SVM, LDA, NB, and KNN. The dataset was split into a 70% training and 30% testing setup, and the results in terms of accuracy are presented in Table 5. Initially, the classifiers were trained using only θ_T^{Max}, and θ_T^{Min} within each segmented window, as the importance of using the thigh angles in HAR was reported in previous studies [41], [42]. As shown in Table 5, the KNN classifier achieved the highest accuracy of 92.03%. However, this level of precision was insufficient for real-time implementation as the features from the thigh were not enough to give sufficient information for satisfactory performance. To improve the performance, features from the foot were included in the training set. The inclusion of these features significantly enhanced the level of classification precision. The classifiers were shown to achieve the following accuracies: 99.90% (SVM), 99.79% (LDA), 100% (NB), and 100% (KNN). While the 100% accuracy achieved by NB and KNN is promising, this result should be interpreted with caution due to the small training sample (10 young adults for training the model), which may lead to optimistic estimates and potential overfitting.

Both the NB and the KNN classifiers performed well and make them ideal candidates for real-time implementation. In normal activity mode, during which young adults climbed stairs with regular alternating leg movement, the classifiers achieved near-perfect accuracy. In the NAL pattern, however, the classifiers were less precise with more overlap between the feature clouds for normal and NAL-SN. In the NAL pattern, classifiers trained with the features from the thighs were less efficient. The NB classifier was the best in this context. However, when features from the feet were added, the KNN classifier performed better, achieving an accuracy of 96.64%. While this was lower than in normal mode, it was still acceptable for practical use. Considering the results from both normal and NAL patterns, the KNN classifier was selected as the most practical for implementation in the real-time application. With a very high rate of accuracy in both activity modes and ease in implementation, it was the best option for the smartphone application that was developed.

E. REAL-TIME EXPERIMENT

The KNN classifier was deployed in the application to evaluate the real-time performance of the developed app for activity detection. The confusion matrix for all activities performed by group 2 (young adults) is presented in Fig. 10. The detection accuracy for walking reached 100%, while errors were more often during the SA, where the model occasionally confused it with SD. The overall detection accuracies for standing, walking, stair ascending, stair descending, and sitting were 99.8%, 100%, 97.2%, 98.8%, and 99.8%, respectively. For the non-alternating leg (NAL) pattern of SN, the confusion matrix for detection accuracy is shown in Fig. 11. Since the NAL model focuses on differentiating between the normal pattern and the NAL pattern of SN, only stair-related activities were used for evaluation. The detection accuracies for stair ascending, NAL stair ascending, stair descending, and NAL stair descending were 95.0%, 94.0%, 96.68%, and 93.3%, respectively.

The performance of the model was also analyzed for older adults (group 5) performing normal activity patterns as illustrated in the confusion matrix in Fig. 12. Similar to young adults, detection of walking was perfect in terms of accuracy. ST, W, SA, SD, and SI were detected with detection accuracies of 100%, 100%, 98.3%, 99.3%, and

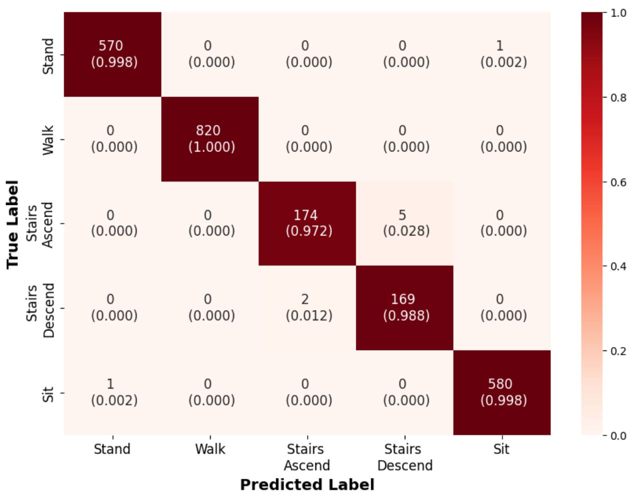

FIGURE 10. Confusion matrix for stand, sit, walk, stairs ascend, and stairs descend for group 2 with young adults with normal patterns of W and SA/SD.

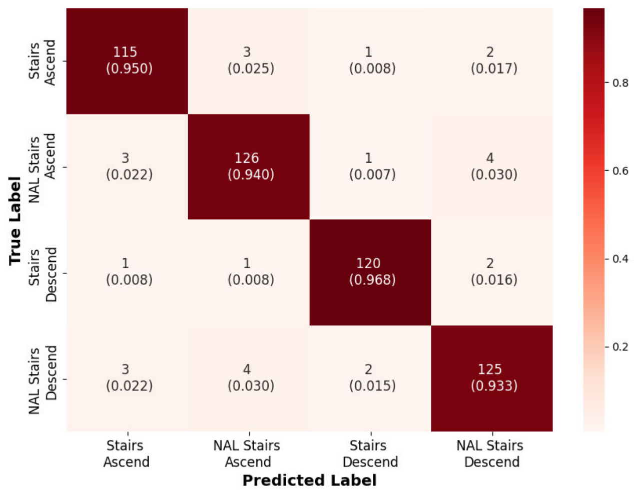

FIGURE 11. Confusion matrix for stairs ascend and descend for group 4 with young adults to have a non-alternating leg (NAL) pattern of SA/SD and comparing them to normal patterns.

99.7%, respectively. To evaluate the robustness of the model in detecting the NAL pattern in older adults, the confusion matrix is illustrated in Fig. 13. Similar to Fig. 11, stair-related activity alone was utilized in this study. Normal ascending and descending stairs were detected with detection accuracies of 95.3% and 93.9%, respectively, while NAL-SA and NAL-SD were detected with detection accuracies of 93.6% and 92.1%, respectively. These results illustrate the detection accuracy of the model in various age groups and activity patterns with particularly robust detection in discriminating between normal and NAL-SN patterns.

F. PARTICIPANT WITH NAL

One participant with leg (NAL) pattern participated in our study, whose data were not included in the final results in Fig. 13. They had Osteopenia and a toe injury, making them utilize their left leg as the leading leg during SA and the right leg during SD consistently. Due to their condition, data collection during SD was not feasible. The model demonstrated high accuracy in detecting SA, correctly classifying 20 out of 21 collected samples (95.2%), with only one misclassification as normal SD. In addition, for ST, SI, and W, the model was perfectly correct (100%), accurately classifying all data samples.

V. DISCUSSION

A. BIOMECHANICS FEATURES

Statistical analysis revealed no significant differences in the selected biomechanical features between older and young adults across activities. This finding can explain the applicability of the model trained and created by young adults to older-adult participants. The analysis of activity × age interaction term showed significant differences between young and older adults in θ_F^{Max} and $_F^{Min}$ for the W and $_F^{Max}$ for the SD conditions. However, the model still maintained a high level of accuracy for older-adult participants, demonstrating its feasibility for implementation in this population. The foot features ($_F^{Max}$ and $_F^{Min}$) significantly changed during stair negotiation (SA and SD) compared to walking (W); however, a significant difference between the SA and SD was only observed in θ_F^{Min}. As previously reported [41], [42] and confirmed in this study, the thigh features of $_T^{Max}$ and $_T^{Max}$ played a crucial role in the activity detection model as they both significantly changed across the three activities of the W, SA, SD. Thus, the statistical results suggest that combining thigh and foot features enhances the model's robustness, improving its accuracy in distinguishing the three activities.

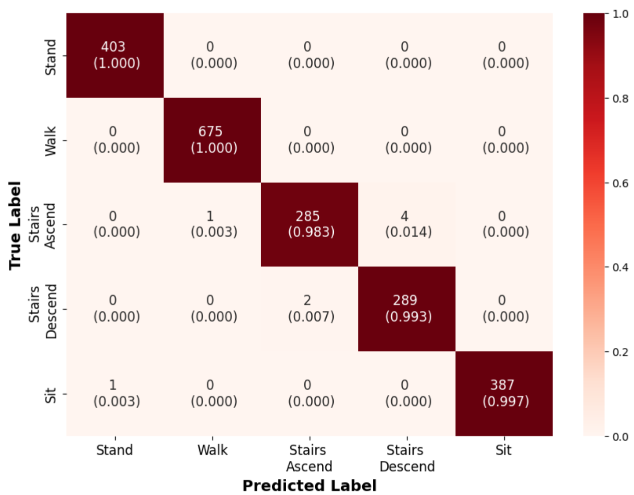

FIGURE 12. Confusion matrix for stand, sit, walk, stairs ascend, stairs descend for group 5 that included older adults with normal patterns of W and SA/SD.

B. OFFLINE EXPERIMENT

Offline experiments were conducted to assess the model's performance using data collected from young adult groups

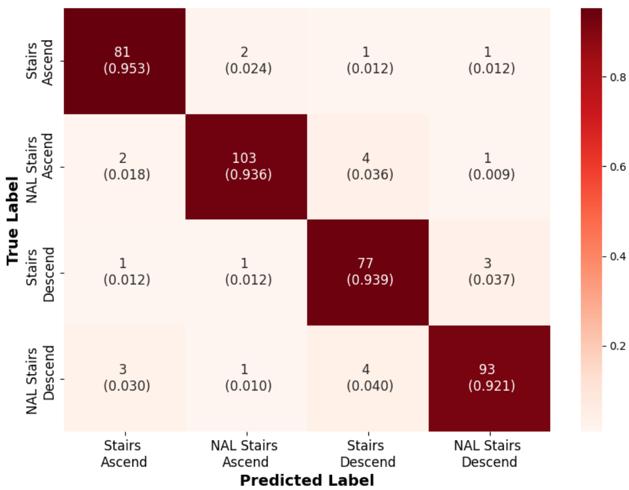

FIGURE 13. **Confusion matrix for stairs ascend and descend for group 6 that included older adults with a non-alternating leg (NAL) pattern of SA/SD and comparing the results with the normal patterns.**

performing walking, sitting, standing, and both normal and non-alternating leg patterns during stair negotiation. The KNN and NB classifiers achieved 100% accuracy across all the activities' test data for the normal SN patterns. While these results are promising, they are based on a relatively small sample size, and the classifiers' accuracy may decrease with a larger and more diverse population. In particular, the perfect accuracy may reflect optimistic performance due to potential overfitting to the small training set. Our dataset of ten young participants, with sufficient activity duration and variability in physical attributes such as height, weight, and gender, provided a reasonable foundation for training the model applicable to older adults.

The results also indicated that using solely the thigh features was insufficient for achieving acceptable accuracy. Incorporating additional features from the foot significantly improved the performance, demonstrating that a combination of thigh and foot data with simple max and min variables could successfully detect the intended activities. We found that using fewer features reduced the model's accuracy, particularly for real-time applications, while adding more features would increase computational cost without substantial benefits. Thus, the selected features could achieve a balance between computational efficiency and classification performance.

For the NAL patterns, the offline results demonstrated that the model remained effective with the selected features. Although the accuracy for detecting NAL-SA activities was lower than that of normal activities, the reduction was relatively modest. For example, the accuracy of the KNN classifier decreased by 3.36% (from 100% to 96.64%), while the accuracy of the NB classifier decreased by 3.79% (from 100% to 96.21%). These reductions were anticipated due to the increased overlap between the data points representing normal SN and NAL-SN, particularly for descending stairs. It should be noted that while larger population data sets may decrease the classification accuracies, the current sample provides sufficient variability in movement patterns and physical characteristics to validate the model. Overall, the model could successfully classify SN activities, including the NAL-SN patterns, which makes it applicable for older adults who demonstrate non-alternating stair negotiation. Although all classifiers performed similarly (see Table 5), the KNN classifier was selected for real-time deployment due to its slightly better performance and straightforward implementation.

C. REAL-TIME EXPERIMENT

New participants (groups 2 and 4) were recruited to test the developed models in the real-time experiments. The confusion matrix in Fig. 10 demonstrates high performance of the classifier for group 2 in detecting normal W and SA patterns. Walking was detected with 100% precision, with no misclassification in differentiating walking and stairs negotiation. Most errors were observed in SN due to the confusion between ascending and descending stairs, however, these errors were negligible (2.8% and 1.2% for SA and SD, respectively). The errors are due to the similarities of the thigh features during SA and SD activities. A single instance of confusion occurred between sitting and standing. This misclassification may stem from variability in sitting postures, where the thigh and foot angles can overlap with ST leading to the observed error.

For young adults simulating NAL-SN, observed in some older adults or those with disabilities, the model achieved an overall accuracy of 94% as shown in Fig. 11. As was expected in the Method Sec II-G, the accuracy for NAL patterns model is lower compared to the normal patterns model because of the overlap between NAL and normal features clusters (Fig. 7). The ability to distinguish between normal and NAL patterns was evident for both the SA and SD, however, the classifier performance was slightly better for the SA. These results highlight the model's robustness in detecting distinct SN patterns, even under NAL conditions. The most repetitive error with the model was the confusion of the NAL-SD with NAL-SA. As the model's ultimate goal is implementation for older adults, group 5 results provided further validation. Despite variability of older-adult participants' FGA scores (ranging from 13 to 30), the model achieved an acceptable accuracy of 99.5% (see Fig. 12). While this suggests that the classifier can detect activities across a range of FGA scores, correlation analysis revealed no statistically significant trend between FGA score and model accuracy ($r = 0.30$, $p = 0.55$). Moreover, the participant with the lowest FGA score (13) achieved a comparable accuracy (98.7%) to those with higher scores. Nonetheless, given the limited sample size, these results should be interpreted with caution, and further validation in larger and more clinically diverse populations, particularly those with low FGA, is recommended.

For group 6, which included older adults instructed to mimic NAL-SN, the model achieved an overall accuracy of 94% (Fig. 13) similar to group 4 results with young participants performing the same tasks. Similarly, the main errors were due to the confusion between the normal and NAL stair negotiation tasks, i.e., the misclassification of the NAL-SD and NAL-SA with normal SA and SD. These similarities indicate that the age group did not affect the accuracy of detection for the NAL movements. The results demonstrate the model's applicability for older adults and its ability to handle complex NAL-SN movements during real-time activity detection. It is worth noting that the model successfully distinguishes between normal and NAL SA and SD. However, distinguishing between different activities, regardless of pattern type, could be performed with greater accuracy. This is promising because the developed model can detect the presence of NAL in older adults, making it useful for home-based gait diagnosis. As mentioned earlier, one participant with NAL-SN patterns participated in the study with the model

D. THE ROLE OF RAMPS

To enhance the robustness of W detection, portions of the data acquisition were collected with a 4° ramp in order to simulate uphill and downhill walking. This was included in preparation for real-life environments with varying terrains. The same ramp was also applied during testing, and the results were that there was no misclassification between walking with SN or SD. This indicates that the model is able to accurately detect W even with a normal ramp, enabling consistent performance in real-life environments.

E. THE ROLE OF HANDRAIL

For safety and convenience for young and older adults, handrails were allowed for use by the subjects if required. This also allowed us to design a flexible system that could accurately classify activity even in the presence of handrails, particularly in the use of stairs or ramps. Two subjects in group 6 made use of handrails during SN, and the findings were that the use of handrails did not impact the accuracy in the classification.

F. EFFECT OF IMU ERRORS AND NOISE

The orientation error of the IMUs, a maximum of 2° under dynamic conditions as reported by the manufacturer, is not expected to significantly affect the model's performance. Such a level of error is small and within the inherent variability of the extracted biomechanical features, for which the model's performance is high. As shown in Table 7., all the standard deviations of the biomechanical features are greater than 2°. Furthermore, with regard to toe-off detection, Fig. 14 demonstrates that the angle difference between the actual toe-offs and local minima consistently exceeds the reported error margin (43°), thereby supporting the reliability of the segmentation process. Given that the model is based solely on maximum and minimum orientation angles, these small deviations fall well within the range of inter-class separability. In addition, signal quality analysis using the signal-to-noise ratio (SNR) revealed values exceeding 25 dB across all activities and participants, indicating low noise levels and further validating the robustness of both the segmentation and classification components of the model.

G. COMPARISON WITH OTHER METHODS

Comparison with existing approaches may be challenging due to differences in training and testing sets, recognition targets, and sensor usage. However, Table 6 summarizes studies with equivalent focus in activity recognition like ST, SI, W, and SN, but excluding deep learning approaches and employing biomechanical features. There are studies [44], [60] that report improved accuracy, but their methods generally employ more sensors, more biomechanical features, or more latency in activity recognition. Compared to other methods using only one IMU, our approach exceeded the accuracy reported in [43] and the applicability in real-time in [42]. There were a number of studies that examined powered lower limb prostheses [41], [61] in that population, but they did not consider the patterns in older adults, such as the NAL patterns.

With the deployment of deep learning models, Tang et al. [28] employed shallow hierarchical-split (HS) blocks with at least three IMUs. However, their use of a fixed sliding window segmentation strategy introduced a delay of approximately 132 ms due to the windowing mechanism. Ali and Abdelhafeez [23] combined CNN and LSTM models, demonstrating their potential for real-time applications; however, the model was not deployed and tested in a real-time setting. Alawneh et al. [29] used a personalized LSTM model to detect 17 activities with accuracy up to 98.54%. However, the system relies on a large dataset (UniMiB SHAR) and introduces a 0.35-second computational delay due to personalization steps and 3*s* of fixed windowing data.While Akter et al.'s attention-based CNN with CBAM [30] achieved 96.86% accuracy, its dependency on spectrogram transformations, multi-channel IMUs, and fixed 3-second segmentation limits its feasibility for low-latency, mobile-based systems. While HARTH [38] achieved an F1-score of 0.81 using SVM and 161 features, the reliance on fixed windows and high-dimensional input may limit real-time use, especially for edge devices or older adults. In comparison to the model that was deployed on an edge device, Zhou et al. [32] deployed their TinyML on an Arduino Nano, targeting real-time in low power; however, due to the same issue of using the sliding windowing technique, the delay time is about 2s. Our model bridges the gap in the current studies by specifically examining this population and accommodating their specific movement patterns.

In addition, none of these studies involved testing older adults. The most critical advantage of our system is that it is balanced in terms of latency, accuracy, and practical implementation. Our method is cost-effective and home-based and uses an Android smartphone. In contrast, other cost-effective systems with Raspberry Pi [41], [61] are less practical for home implementation in most cases and may lack the same level of performance. Although the model

TABLE 6. Comparison between the presented model and other recent methods.

Author	Feature	Activities	Number of IMUs	Instrumented limb	Classifier	Accuracy	Delay time, if real-time	Deployment
Young 2016 [44]	Max, min, mean, sd of lower limb angles	Level walk, ramps, stairs	13 Potentiometers and encoders, axial load, IMU	IMU on shank, Potentiometers and encoders on knee and ankle, and load cell on foot	LDA + DBN	99.5%	300 ms	External desktop computer
Chinimilli 2017 [63]	Intelligent fuzzy inference (IFI)	Level walk, sit, stand, stairs, jog	4 IMU 2 Smart shoes	Thigh, shank, foot	RFS	99.1%	Update time 2000 ms	MATLAB (for offline operating)
Martínez-Hernandez 2018 [60], 2018 [56]	Angular velocisy	Level walk, ramps	3 IMU 1 FSR	Thigh, Shank, foot	Adaptive BasIs	99.87%	240 ms	Laptop workstation (For operating the model in real-time)
Bartlett 2018 [42]	A and angular velocity	Level walk, Stairs	1 IMU	Thigh	Phase variable (PV), LDA	98.4%	Not real-time	-
Chinimilli 2019 [43]	Amplitude-Omega	Level walk, uphill, downhill, run	1 IMU	Thigh	SVM, KNN	98.1%	80 ms	Intel Edison
Chinimilli 2019 [43]	Amplitude-Omega	Level walk, stairs, jog	1 IMU	Thigh	SVM, KNN	93.3%	80 ms	Intel Edison
Cheng 2021 [41]	Instantaneous Characteristic Features (ICF)	Walk, stairs, Sit	1 IMU, 1 FSR	IMU on thigh FSR on Foot	KNN – SVM – NB	99.4%	5 ms	Raspberry Pi
Logacjov 2021 [38]	161 statistical features (acceleration)	12 activities	2 IMUs	Thigh and lower back	SVM (best), CNN, BiLSTM	F1- score: 0.81	-	-
Ali 2022 [23]	Acceleration (value, statistical), angles	Walk, stairs, sit, laying, stand	A smartphone	Waist	CNN + LSTM	Offline: 98%	-	-
Tang 2022 [28]	Acceleration, gyro, magnetometer	Walk, stairs, sit, jog	At least 3	Dominant hand, chest, ankle	CNN	99.02%	132 ms	Raspberry Pi
Akter 2023 [30]	6 channel of acceleration and Gyro	18 (KU-HAR) Walk, run, stairs, lying, jump	Wirst mounted IMU	Wirst	CNN + CBAM) (Attention-based))	96.86%	3000 ms of window	-
Alwaneh 2023 [29]	3-axial time-series data	17 activities of types of, walk, run, fall, sit, and jump	Smartphone IMU	-	LSTM	98.54%	350 ms	Edge devises
Deng 2023 [33]	Accelerometer, Gyro + + multi-sensor (PAMAP2)	12 activities	Dataset: OPP: 7 IMUs + PAMAP2 with 3 IMUs	Chest, wrist, ankle	CNN with Knowledge	Offline: 99.3%	-	-
Ansah, 2024 [40]	Normalized pitch angle of thigh	Walk, stairs	2 IMU, 2 Smart insole shoes	Thigh, foot	KNN	>97%	Not real-time	-
Bhakta 2025 [61]	Lower-limb powered prostheses	Level walk, ramps, jogging	2 encoders, 3 IMU, 1 loadcell	IMUs on thigh, shank, foot, Encoders on knee and ankle Loadcell on foot	XGBOOST	Offline Error: 5.37% Real-time Error: 19.0%	157 ms	Raspberry Pi 4
Zhou 2025 [32]	Accelerometer, Gyro (6 Channel)	Walk, sit, stand, stairs, jog	1 IMU	Wrist	DeepConv LSTM (TinyML)	98.24%	2000 ms	Arduino Nano 33 BLE (Edge, TinyML)
Our method	Max and min values of thigh and foot	Walk, sit, stairs	2 IMU	Thigh, foot	KNN	Real-time: 99.1% for normal pattern 93.4% for NAL pattern	52 ms	Android smartphone system

by Cheng et al. [41] had slightly higher overall accuracy, it was trained with a larger data set from a previous study using a camera-based motion capture system [62]. Therefore, our study was successful with two IMU and data from 15 participants, which shows the efficacy of our method.

H. LIMITATIONS AND FUTURE WORK

Several limitations in this study need to be addressed in the future. A significant limitation of this study is the small sample sizes used for testing, particularly within the older adult groups. While the model demonstrated high accuracy, including cases with 100% in offline analysis, small sample sizes limit the statistical power of the findings and may overestimate the model's robustness and generalizability. This is particularly important when considering deployment in a broader, more heterogeneous population of older adults. Therefore, future studies with larger and more diverse cohorts are necessary to validate and generalize the findings.

Moreover, although the model could detect the NAL-SN patterns, future studies should investigate the efficacy of the model by recruiting more participants with NAL-SN patterns such as individuals with Parkinson's disease. Another limitation concerns the real-time segmentation method, which employs adaptive windowing based on toe-off detection. Future studies should explore advanced segmentation techniques to enhance the model's performance, especially for older adults with irregular step timing. The current threshold criteria were derived from a limited sample and may not retain the same level of accuracy in broader, more diverse populations. Expanding the criteria or using other adaptive methods may be necessary to enhance generalizability. Furthermore, the long-term usability of the system should be evaluated to determine its effectiveness for home-based use by older adults.

VI. CONCLUSION

This study presented a real-time HAR system using minimal lower-limb biomechanical features obtained from thigh and foot mounted IMUs. The model was trained on young adults and tested on both young and older adults, demonstrating its generalizability.

The model was trained to incorporate NAL-SN patterns to accommodate older adults among others with this mobility limitation. The results highlight the feasibility of deploying this lightweight HAR system on smartphones. Unlike deep learning approaches that require extensive datasets for training, the proposed model emphasizes simplicity and computational efficiency, making it a practical physics-based classifier for real-time applications. The method achieved high accuracy in classifying activities and detecting as well as distinguishing between normal and NAL-SN patterns.

CONFLICT OF INTEREST

None of the authors have a conflict of interest to disclose.

APPENDIX A

The two thresholds used for toe-off detection in our segmentation process, a minimum time threshold of 0.4s

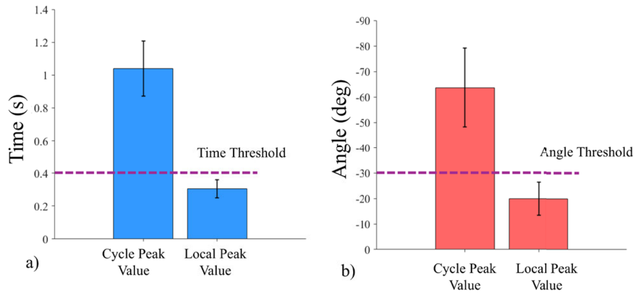

FIGURE 14. **The distribution of time (a) and angle (b) differences between consecutive actual toe-offs with cycle peak value (actual toe-off candidates) shown in blue bar plots and the difference with local peak value (false toe-off candidates), shown in red bar plots based on data from young participants. Clear separations are visible in both plots, supporting the use of the minimum time threshold of a) 0.4s and b) −30° for angle to reject false detections.**

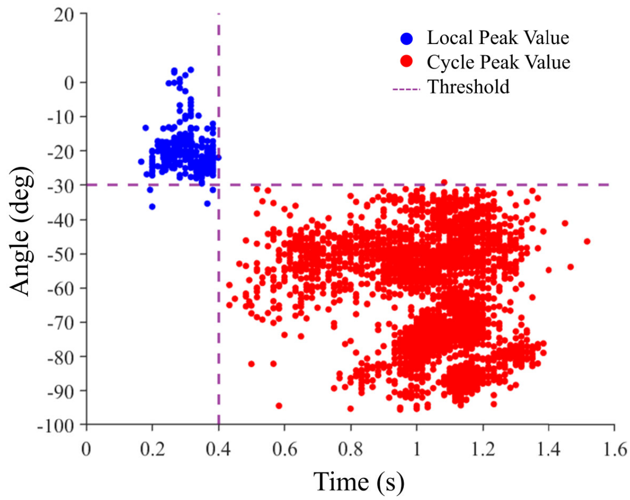

FIGURE 15. **Comparison of the foot angle and time interval features for the actual toe-off events (cycle peak value) versus local minima in young participants. The clear distinction between the two groups supports the selected thresholds of −30° for the foot angle and 0.4s for the time difference.**

between consecutive events and a foot angle threshold of −30°, were empirically derived from the training data. While similar thresholds are discussed in the literature to help identify toe-off events and minimize false detections caused by local minima in the IMU signals, we chose to calibrate our values based on the specific characteristics of our dataset and system implementation to ensure optimal performance in real-time settings. During preliminary analysis, we observed that local minima in the foot angle signal were particularly observed during stair negotiation activities (especially stair descent as shown in Fig. 3), while level walking produced cleaner, more distinguishable toe-off events. Therefore, the thresholds were primarily validated for robustness in complex movement scenarios like stair negotiation, which presented a greater challenge for accurate segmentation.

To empirically support our threshold selection, Figs. 14 and 15 illustrate how actual toe-off events differ from the local peaks, i.e., false toe-off events. Fig. 14 shows the bar plots of the temporal (a) and angular (b) differences of the actual toe-off events with the cycle peaks, which we intended to detect as actual toe-offs, and the local peaks, which we intended to avoid as false toe-offs. Fig. 15 demonstrates the combinations of both plots of Fig.14 (a) and (b) for the angle and time values, distinguishing the cycle and local peaks. These visualizations demonstrate a clear separation between true and false events, guiding our selection of a −30° angle threshold and a 0.4s time threshold values, which fell near the boundary between the clusters. The broader ranges of observed separation were approximately [0.4s, 0.8s] (Fig.14 (a)) for time and [−25°, −45°] (Fig. 14 (b)) for angle, when these two measures are considered separately.

We confirm these thresholds by conducting statistical analysis using paired-sample and one-sample t-tests. The results of the paired-sample t-test showed highly significant differences ($p < 0.0001$) between the distributions of actual toe-offs and local minima in both angle and time domains. Additionally, each distribution was significantly different from the selected threshold values using a one-sample t-test ($p < 0.0001$). These findings validated the thresholds' ability to discriminate between actual and false events.

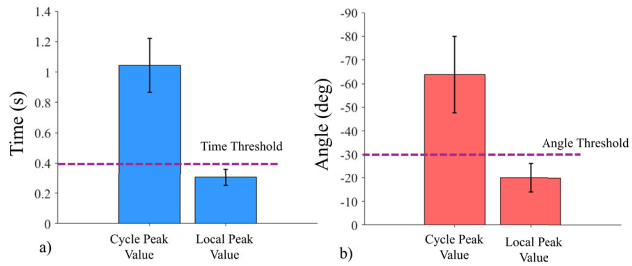

FIGURE 16. **The distribution of time (a) and angle (b) differences between consecutive actual toe-offs with cycle peak value (actual toe-off candidates) shown in blue bar plots and the difference with local peak value (false toe-off candidates), shown in red bar plots based on data from older-adult participants. Similar to the younger group, the results demonstrate clear temporal and angular separations between the actual toe-offs and local minima, validating the generalizability of a) the 0.4s time and b) −30° of angle threshold.**

Finally, we evaluated the generalizability of these thresholds found by the data of young participants by applying them to the older-adult participants' data. Figs. 16 and 17 are similar to Figs. 14 and 15, respectively, present the same analyses for this group and reveal similar separation patterns between the gait cycle and local peaks. Statistical analyses again confirmed significant distinctions between the two peak groups and significant differences between each group and the thresholds ($p < 0.0001$). The older-adult participants' results further support that the thresholds derived from young participants' data retained their discriminative power across age groups.

Regarding walking speed sensitivity, it is important to note that during data collection, participants performed walking and stair activities at both self-selected and fast speeds. This design ensured that the thresholds were exposed to natural ranges of gait speed variability. The consistent performance of the segmentation algorithm across these different speeds

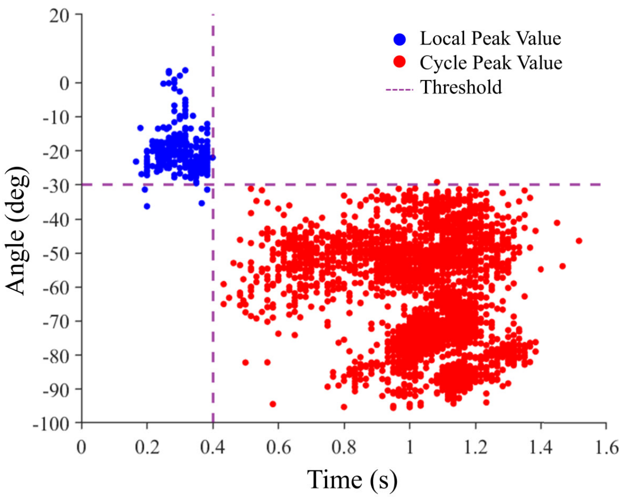

FIGURE 17. Comparison of the foot angle and time difference features for the actual and local (false) toe-off candidates in older adults (part of the testing group). The clear separation supports the sustained effectiveness of the segmentation thresholds across age groups.

and participant ages supports the robustness of our chosen threshold values.

In summary, although the thresholds were originally derived from training data of young adults, their effectiveness was validated through both visualization and statistical analysis for older adults and across varied walking speeds. This confirms that these thresholds are applicable not only for the training cohort but also generalize well across populations and movement conditions. However, it should be noted that in a larger and more diverse population with greater variability in speed and movement patterns, the accuracy of the current criteria might decrease, necessitating the addition of further segmentation parameters. The selected criteria in this study were chosen as a trade-off between computational efficiency and classification performance, tailored to the constraints of our limited sample size and target population.

APPENDIX B

Regarding the errors of the sensors, in our study, we utilized the orientation output from the Movella DOT sensors, which is generated using the device's onboard XKFCore Kalman filter-based sensor fusion algorithm (Movella Inc. 2023). This algorithm combines raw accelerometer, gyroscope, and magnetometer data to produce drift-free 3D orientation estimates, optimized specifically for human motion tracking. According to the manufacturer's specifications, the Movella DOT provides orientation accuracy of 0.5° RMS for inclination and 1.0° RMS for heading under static conditions, and 1.0°/ 2.0° RMS for inclination and heading, respectively, under dynamic conditions. Our features for the model are based solely on thigh and foot orientation angles, and not from raw IMU signals. The internal noise characteristics of individual sensors (e.g., accelerometer noise or gyroscope bias) have already been accounted for and compensated within the sensor fusion process.

It should be noted that there are other off-the-shelf IMUs (e.g., Movella DOT used here, APDM Opal, MetaMotion R, etc.) with similar sensor fusion algorithms that utilize accelerometers, gyroscopes, and magnetometers to accurately estimate orientation (including quaternions and Euler angles) with low noise. Given the availability and prevalence of such IMUs, our proposed method, including both the algorithm and selected features, is designed for use with these IMUs, anticipating their increasing adoption by researchers.

First, we quantified the level of noise with the collected data and calculated the Signal-to-Noise Ratio (SNR). SNR is a critical metric that compares the power of the desired signal to the power of the unwanted noise, typically expressed in decibels (dB). A higher SNR value indicated a cleaner signal with less interference from noise. The general formula for SNR in decibels is:

$$SNR_{dB} = 10 \cdot \log_{10}\left(\frac{P_{\text{signal activity}}}{P_{\text{noise}}}\right) \tag{1}$$

where,

- $P_{\text{signal activity}}$ represents the power of the true underlying motion signal.
- P_{noise} represents the power of the inherent sensor noise and other undesirable fluctuations.

For practical application to IMU data, where the true signal and noise components are not directly separable, an estimation approach is employed: The noise power of each IMU sensor (foot and thigh) was estimated from the standing period within the collected data. During this stationary period, it is assumed that there is no intended anatomical motion, and therefore, any observed fluctuations in the recorded angle are primarily attributable to sensor noise and minor physiological sway.

$$P_{\text{noise}} = \text{mean}\left((\text{angle data[standing indices]})^2\right) \tag{2}$$

For each specific dynamic activity (Walking, Upstairs, Downstairs), the total power of the angle signal was calculated. This total power includes both the power of the actual motion and the underlying sensor noise present during that activity.

$$P_{\text{total activity}} = \text{mean}\left((\text{angle data[othe activity indices]})^2\right) \tag{3}$$

The power of the true motion signal for each activity was then estimated by subtracting the previously determined global noise power from the total power of that activity's segment. This assumes that the noise is additive and its power remains consistent across different activities.

$$P_{\text{signal activity}} = P_{\text{total activity}} - P_{\text{noise}} \tag{4}$$

This detailed process allowed for a quantitative evaluation of the signal quality of the foot and thigh angle data, enabling a comparative assessment of noise levels during various dynamic movements.

We considered the criteria reported in a study [57], as SNR values for IMU, above 25 dB indicate high-quality data, and

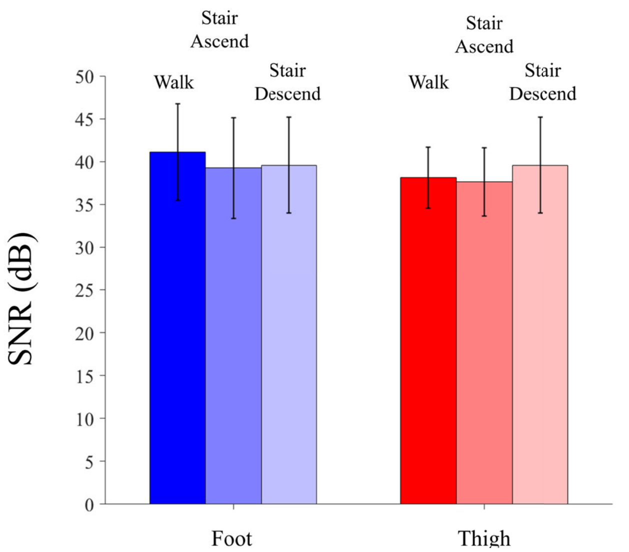

FIGURE 18. Signal-to-noise ratio (SNR) of the IMU angle signals from thigh and foot sensors during walking, stair ascent, and stair descent. All values exceeded 25 dB, indicating high-quality signals across all participants and activities.

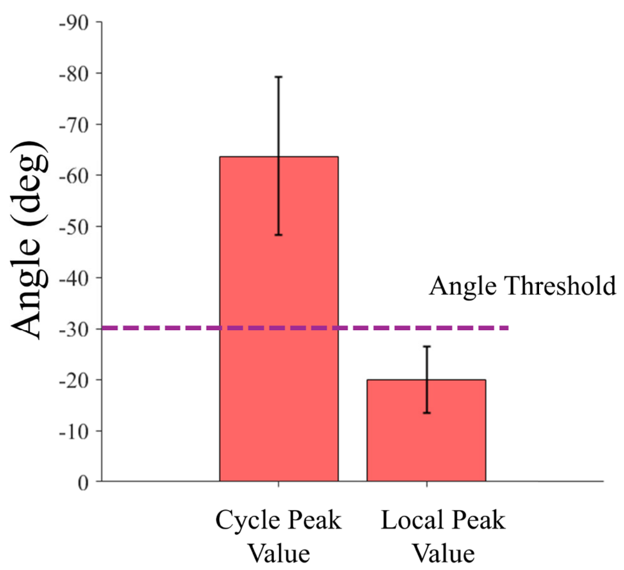

FIGURE 19. The distribution of angles between consecutive actual toe-offs with cycle peak value (actual toe-off candidates) shown in red bar plots based on data from young participants. Clear separations are visible in both plots, supporting the use of the minimum time threshold of 30° for angle to reject false detections.

below 10 dB may reflect poor signal quality. The SNR for all the data, including training and testing data, was calculated and is shown in Fig. 18. The SNR values for all participants across walking, stair ascent, and stair descent exceeded 25 dB for both thigh and foot IMUs. This confirms that the IMU signals used in this study were of high quality, with minimal noise interference, and did not compromise the accuracy or stability of the segmentation or classification model.

Second, regarding how the sensor's dynamic error affects the segmentation and classification model: (I) The segmentation window is determined by detecting the actual toe-off moments, defined as the minimum foot angle within a gait cycle (i.e., cycle peak value) in the orientation signal. According to the manufacturer, the maximum expected dynamic orientation error is $\pm 2^{\circ}$. To assess whether this dynamic error affects toe-off detection and causes a detection confusion between cycle peaks (actual toe-offs) and local peaks (false toe-offs), we compared the distribution of the actual toe-off values (i.e., cycle minima) and local peaks. As shown in Fig. 19, the mean $\pm$ standard deviation of the actual toe-offs was $-23.06 \pm 6.21^{\circ}$, while the local minima had a mean of $-63 \pm 16.20^{\circ}$. This clear separation shows that even a 2° error is negligible in affecting segmentation accuracy.

(II) In terms of activity classification, the model relies on the maximum and minimum orientation values of the thigh and foot in each segment. Fig. 9 and Table 7 show that these biomechanical features are significantly different across walking, stair ascent, and stair descent ($p < 0.001$ for all comparisons). While some overlap exists due to natural variability, a 2° orientation error falls well within the margin of separation between classes (please note that all the standard deviations in Table 7 are greater than 2°) and it is unlikely to degrade model accuracy in any meaningful way.

In summary, since our model relies solely on orientation outputs, the reported maximum dynamic error of approximately 2° from the IMUs is unlikely to meaningfully affect the detection of toe-off events or the extraction of peak values within each segmented window. Additionally, our SNR analysis confirmed that the orientation signals were of high quality, and the observed variability in the data did not suggest that noise had a significant impact on the model's performance. It is important to note that if other researchers aim to develop similar detection algorithms using IMUs with different sensor fusion techniques, the noise analysis provided in this study may not be transferable.

TABLE 7. The biomechanical features, such as the mean and standard deviation.

Feature	Walk	Stairs Ascend	Stairs Descend
Max. thigh (deg)	33.46 ± 5.38	54.03 ± 5.20	39.61 ± 5.94
Min. thigh (deg)	-13.89 ± 3.54	-2.44 ± 3.17	10.60 ± 4.25
Max. foot (deg)	28.54 ± 4.69	-0.73 ± 4.64	-1.55 ± 2.49
Min. foot (deg)	-69.65 ± 11.27	-48.20 ± 6.32	-52.33 ± 4.93

REFERENCES

[1] S. Mazilu, U. Blanke, M. Hardegger, G. Tröster, E. Gazit, and J. M. Hausdorff, "GaitAssist: A daily-life support and training system for Parkinson's disease patients with freezing of gait," in *Proc. SIGCHI Conf. Hum. Factors Comput. Syst.*, Apr. 2014, pp. 2531–2540.

[2] S. Patel, H. Park, P. Bonato, L. Chan, and M. Rodgers, "A review of wearable sensors and systems with application in rehabilitation," *J. NeuroEng. Rehabil.*, vol. 9, no. 1, pp. 1–17, Dec. 2012.

[3] P. Rashidi and D. J. Cook, "Keeping the resident in the loop: Adapting the smart home to the user," *IEEE Trans. Syst., Man, Cybern., A, Syst. Hum.*, vol. 39, no. 5, pp. 949–959, Sep. 2009.

[4] S. J. Preece, J. Y. Goulermas, L. P. J. Kenney, D. Howard, K. Meijer, and R. Crompton, "Activity identification using body-mounted sensors—A review of classification techniques," *Physiolog. Meas.*, vol. 30, no. 4, pp. R1–R33, Apr. 2009.

[5] A. Poulose, J. H. Kim, and D. S. Han, "HIT HAR: Human image threshing machine for human activity recognition using deep learning models," *Comput. Intell. Neurosci.*, vol. 2022, pp. 1–21, Oct. 2022.

[6] F. Demrozi, G. Pravadelli, A. Bihorac, and P. Rashidi, "Human activity recognition using inertial, physiological and environmental sensors: A comprehensive survey," *IEEE Access*, vol. 8, pp. 210816–210836, 2020.

[7] F. Alam, P. Pławiak, A. Almaghthawi, M. R. C. Qazani, S. Mohanty, and A. R. Alizadehsani, "NeuroHAR: A neuroevolutionary method for human activity recognition (HAR) for health monitoring," *IEEE Access*, vol. 12, pp. 112232–112248, 2024.

[8] T. Rowland, "Effectiveness of interventions to promote physical activity in children and adolescents: Systematic review of controlled trials," *Yearbook Sports Med.*, vol. 2009, pp. 286–287, Jan. 2009.

[9] G. Baker and N. Mutrie, "Are pedometers useful motivational tools for increasing walking in sedentary adults," in *Proc. 6th Int. Conf. Walking 21st Century*, 2005.

[10] B. M. V. Guerra, E. Torti, E. Marenzi, M. Schmid, S. Ramat, F. Leporati, and G. Danese, "Ambient assisted living for frail people through human activity recognition: State-of-the-art, challenges and future directions," *Frontiers Neurosci.*, vol. 17, Oct. 2023, Art. no. 1256682.

[11] M. F. Trujillo-Guerrero, S. Román-Niemes, M. Jaén-Vargas, A. Cadiz, R. Fonseca, and J. J. Serrano-Olmedo, "Accuracy comparison of CNN, LSTM, and transformer for activity recognition using IMU and visual markers," *IEEE Access*, vol. 11, pp. 106650–106669, 2023.

[12] W. Guo, S. Yamagishi, and L. Jing, "Human activity recognition via Wi-Fi and inertial sensors with machine learning," *IEEE Access*, vol. 12, pp. 18821–18836, 2024.

[13] S. Seenath and M. Dharmaraj, "Conformer-based human activity recognition using inertial measurement units," *Sensors*, vol. 23, no. 17, p. 7357, Aug. 2023.

[14] O. Steven Eyobu and D. S. Han, "Feature representation and data augmentation for human activity classification based on wearable IMU sensor data using a deep LSTM neural network," *Sensors*, vol. 18, no. 9, p. 2892, Aug. 2018.

[15] W. Tao, H. Chen, M. Moniruzzaman, M. C. Leu, Z. Yi, and R. Qin, "Attention-based sensor fusion for human activity recognition using IMU signals," 2021, *arXiv:2112.11224*.

[16] V. Bianchi, M. Bassoli, G. Lombardo, P. Fornacciari, M. Mordonini, and I. De Munari, "IoT wearable sensor and deep learning: An integrated approach for personalized human activity recognition in a smart home environment," *IEEE Internet Things J.*, vol. 6, no. 5, pp. 8553–8562, Oct. 2019.

[17] M. Nassajpour, M. Shuqair, A. Rosenfeld, M. I. Tolea, J. E. Galvin, and B. Ghoraani, "Objective estimation of m-CTSIB balance test scores using wearable sensors and machine learning," *Frontiers Digit. Health*, vol. 6, Apr. 2024, Art. no. 1366176.

[18] M. Nassajpour, M. Shuqair, A. Rosenfeld, M. I. Tolea, J. E. Galvin, and B. Ghoraani, "Smartphone-based balance assessment using machine learning," in *Proc. 46th Annu. Int. Conf. IEEE Eng. Med. Biol. Soc. (EMBC)*, Jul. 2024, pp. 1–4.

[19] L. Lu, C. Zhang, K. Cao, T. Deng, and Q. Yang, "A multichannel CNN-GRU model for human activity recognition," *IEEE Access*, vol. 10, pp. 66797–66810, 2022.

[20] I. U. Khan, S. Afzal, and J. W. Lee, "Human activity recognition via hybrid deep learning based model," *Sensors*, vol. 22, no. 1, p. 323, Jan. 2022.

[21] M. H. Arshad, M. Bilal, and A. Gani, "Human activity recognition: Review, taxonomy and open challenges," *Sensors*, vol. 22, no. 17, p. 6463, Aug. 2022.

[22] S. Ek, F. Portet, and P. Lalanda, "Transformer-based models to deal with heterogeneous environments in human activity recognition," 2022, *arXiv:2209.11750*.

[23] A. M. Ali and A. Abdelhafeez, "DeepHAR-Net: A novel machine intelligence approach for human activity recognition from inertial sensors," *Sustain. Mach. Intell. J.*, vol. 1, p. 1, Nov. 2022.

[24] F. Ordóñez and D. Roggen, "Deep convolutional and LSTM recurrent neural networks for multimodal wearable activity recognition," *Sensors*, vol. 16, no. 1, p. 115, Jan. 2016.

[25] Y.-H. Tseng and C.-Y. Wen, "Hybrid learning models for IMU-based HAR with feature analysis and data correction," *Sensors*, vol. 23, no. 18, p. 7802, Sep. 2023.

[26] S. AlKharji, A. Alteneiji, and K. Poon, "IMU-based human activity recognition using machine learning and deep learning models," in *Proc. 6th Int. Conf. Signal Process. Inf. Secur. (ICSPIS)*, Nov. 2023, pp. 62–66.

[27] H. Kwon, G. D. Abowd, and T. Plötz, "Complex deep neural networks from large scale virtual IMU data for effective human activity recognition using wearables," *Sensors*, vol. 21, no. 24, p. 8337, Dec. 2021.

[28] Y. Tang, L. Zhang, F. Min, and J. He, "Multiscale deep feature learning for human activity recognition using wearable sensors," *IEEE Trans. Ind. Electron.*, vol. 70, no. 2, pp. 2106–2116, Feb. 2023.

[29] L. Alawneh, M. Al-Ayyoub, Z. A. Al-Sharif, and A. Shatnawi, "Personalized human activity recognition using deep learning and edge-cloud architecture," *J. Ambient Intell. Humanized Comput.*, vol. 14, no. 9, pp. 12021–12033, Sep. 2023.

[30] M. Akter, S. Ansary, M. A.-M. Khan, and D. Kim, "Human activity recognition using attention-mechanism-based deep learning feature combination," *Sensors*, vol. 23, no. 12, p. 5715, Jun. 2023.

[31] Q. Mascret, M. Bielmann, C.-L. Fall, L. J. Bouyer, and B. Gosselin, "Real-time human physical activity recognition with low latency prediction feedback using raw IMU data," in *Proc. 40th Annu. Int. Conf. IEEE Eng. Med. Biol. Soc. (EMBC)*, Jul. 2018, pp. 239–242.

[32] H. Zhou, X. Zhang, Y. Feng, T. Zhang, and L. Xiong, "Efficient human activity recognition on edge devices using DeepConv LSTM architectures," *Sci. Rep.*, vol. 15, no. 1, p. 13830, Apr. 2025.

[33] S. Deng, J. Chen, D. Teng, C. Yang, D. Chen, T. Jia, and H. Wang, "LHAR: Lightweight human activity recognition on knowledge distillation," *IEEE J. Biomed. Health Informat.*, vol. 28, no. 11, pp. 6318–6328, Nov. 2024.

[34] T. Sziburis, M. Nowak, and D. Brunelli, "Instance-based learning with prototype reduction for real-time proportional myocontrol: A randomized user study demonstrating accuracy-preserving data reduction for prosthetic embedded systems," *Med. Biol. Eng. Comput.*, vol. 62, no. 1, pp. 275–305, Jan. 2024.

[35] H. Zhu, J. Guo, Z. Shao, Y. Zhang, Z. Ding, and H. Gong, "Extra-trees for human activity recognition using wearable sensors," in *Proc. Int. Conf. Intell. Transp., Big Data Smart City (ICITBS)*, Mar. 2022, pp. 801–804.

[36] G. De Leonardis, S. Rosati, G. Balestra, V. Agostini, E. Panero, L. Gastaldi, and M. Knaflitz, "Human activity recognition by wearable sensors: Comparison of different classifiers for real-time applications," in *Proc. IEEE Int. Symp. Med. Meas. Appl. (MeMeA)*, Jun. 2018, pp. 1–6.

[37] F. Attal, S. Mohammed, M. Dedabrishvili, F. Chamroukhi, L. Oukhellou, and Y. Amirat, "Physical human activity recognition using wearable sensors," *Sensors*, vol. 15, no. 12, pp. 31314–31338, Dec. 2015.

[38] A. Logacjov, K. Bach, A. Kongsvold, H. B. Bårdstu, and P. J. Mork, "HARTH: A human activity recognition dataset for machine learning," *Sensors*, vol. 21, no. 23, p. 7853, Nov. 2021.

[39] T. Zebin, P. J. Scully, and K. B. Ozanyan, "Evaluation of supervised classification algorithms for human activity recognition with inertial sensors," in *Proc. IEEE SENSORS*, Oct. 2017, pp. 1–3.

[40] S. Ansah, S. Y. Yoon, and D. Chen, "Human motion intention recognition with thigh mounted IMUs," in *Proc. 46th Annu. Int. Conf. IEEE Eng. Med. Biol. Soc. (EMBC)*, Jul. 2024, pp. 1–4.

[41] S. Cheng, E. Bolívar-Nieto, and R. D. Gregg, "Real-time activity recognition with instantaneous characteristic features of thigh kinematics," *IEEE Trans. Neural Syst. Rehabil. Eng.*, vol. 29, pp. 1827–1837, 2021.

[42] H. L. Bartlett and M. Goldfarb, "A phase variable approach for IMU-based locomotion activity recognition," *IEEE Trans. Biomed. Eng.*, vol. 65, no. 6, pp. 1330–1338, Jun. 2018.

[43] P. T. Chinimilli, S. Redkar, and T. Sugar, "A two-dimensional feature space-based approach for human locomotion recognition," *IEEE Sensors J.*, vol. 19, no. 11, pp. 4271–4282, Jun. 2019.

[44] A. J. Young and L. J. Hargrove, "A classification method for user-independent intent recognition for transfemoral amputees using powered lower limb prostheses," *IEEE Trans. Neural Syst. Rehabil. Eng.*, vol. 24, no. 2, pp. 217–225, Feb. 2016.

[45] M. Alizadeh Noghani, M. Shahinpoor, and B. Hejrati, "Design and validation of a smartphone-based haptic feedback system for gait training," *IEEE Robot. Autom. Lett.*, vol. 6, no. 4, pp. 6593–6600, Oct. 2021.

[46] M. A. Noghani, M. T. Hossain, and B. Hejrati, ‘‘Modulation of arm swing frequency and gait using rhythmic tactile feedback,’’ *IEEE Trans. Neural Syst. Rehabil. Eng.*, vol. 31, pp. 1542–1553, 2023.
[47] M. Alizadeh Noghani, E. Sharafian M., B. Sidaway, and B. Hejrati, ‘‘Increasing thigh extension with haptic feedback affects leg coordination in young and older adult Walkers,’’ *J. Biomech.*, vol. 181, Mar. 2025, Art. no. 112525.
[48] V. R. Shah, P. C. Dixon, and A. P. Willmott, ‘‘Evaluation of lower-body gait kinematics on outdoor surfaces using wearable sensors,’’ *J. Biomech.*, vol. 177, Jan. 2024, Art. no. 112401.
[49] G. Sopidis, M. Haslgrübler, and A. Ferscha, ‘‘Counting activities using weakly labeled raw acceleration data: A variable-length sequence approach with deep learning to maintain event duration flexibility,’’ *Sensors*, vol. 23, no. 11, p. 5057, May 2023.
[50] G. Uslu and S. Baydere, ‘‘A segmentation scheme for knowledge discovery in human activity spotting,’’ *IEEE Trans. Cybern.*, vol. 52, no. 7, pp. 5668–5681, Jul. 2022.
[51] C. Bu, L. Zhang, H. Cui, G. Yang, and H. Wu, ‘‘Dynamic inference via localizing semantic intervals in sensor data for budget-tunable activity recognition,’’ *IEEE Trans. Ind. Informat.*, vol. 20, no. 3, pp. 3801–3813, Mar. 2024.
[52] D. Chen, N. Ghoreishi, F. Olugbon, S. Ansah, M.-C. Huang, and Q. Yu, ‘‘Optimal pressure sensor locations in smart insoles for heel-strike and toe-off detection,’’ in *Proc. IEEE Biomed. Circuits Syst. Conf. (BioCAS)*, Oct. 2022, pp. 458–461.
[53] G. Wang, Q. Li, L. Wang, W. Wang, M. Wu, and T. Liu, ‘‘Impact of sliding window length in indoor human motion modes and pose pattern recognition based on smartphone sensors,’’ *Sensors*, vol. 18, no. 6, p. 1965, Jun. 2018.
[54] H. Martha, ‘‘Functional predictors of stair-climbing ability in older adults,’’ *MOJ Gerontology Geriatrics*, vol. 1, no. 5, pp. 115–118, Jul. 2017.
[55] I. Di Giulio, N. D. Reeves, M. Roys, J. G. Buckley, D. A. Jones, J. P. Gavin, V. Baltzopoulos, and C. N. Maganaris, ‘‘Stair gait in older adults worsens with smaller step treads and when transitioning between level and stair walking,’’ *Frontiers Sports Act. Living*, vol. 2, p. 63, Jun. 2020.
[56] U. Martínez-Hernández and A. A. Dehghani-Sanij, ‘‘Adaptive Bayesian inference system for recognition of walking activities and prediction of gait events using wearable sensors,’’ *Neural Netw.*, vol. 102, pp. 107–119, Jan. 2018.
[57] O. Pearl, S. Shin, A. Godura, S. Bergbreiter, and E. Halilaj, ‘‘Fusion of video and inertial sensing data via dynamic optimization of a biomechanical model,’’ *J. Biomech.*, vol. 155, Jun. 2023, Art. no. 111617.
[58] D. M. Wrisley, G. F. Marchetti, D. K. Kuharsky, and S. L. Whitney, ‘‘Reliability, internal consistency, and validity of data obtained with the functional gait assessment,’’ *Phys. Therapy*, vol. 84, no. 10, pp. 906–918, Oct. 2004.
[59] M. Beninato and L. H. Ludlow, ‘‘The functional gait assessment in older adults: Validation through Rasch modeling,’’ *Phys. Therapy*, vol. 96, no. 4, pp. 456–468, Apr. 2016.
[60] U. Martinez-Hernandez, I. Mahmood, and A. A. Dehghani-Sanij, ‘‘Simultaneous Bayesian recognition of locomotion and gait phases with wearable sensors,’’ *IEEE Sensors J.*, vol. 18, no. 3, pp. 1282–1290, Feb. 2018.
[61] K. Bhakta, J. Maldonado-Contreras, J. Camargo, S. Zhou, W. Compton, K. R. Herrin, and A. J. Young, ‘‘Continuous-context, user-independent, real-time intent recognition for powered lower-limb prostheses,’’ *J. Biomech. Eng.*, vol. 147, no. 2, Feb. 2025.
[62] E. Reznick, K. R. Embry, R. Neuman, E. Bolívar-Nieto, N. P. Fey, and R. D. Gregg, ‘‘Lower-limb kinematics and kinetics during continuously varying human locomotion,’’ *Sci. Data*, vol. 8, no. 1, p. 282, Oct. 2021.
[63] P. T. Chinimilli, S. Redkar, and W. Zhang, ‘‘Human activity recognition using inertial measurement units and smart shoes,’’ in *Proc. Amer. Control Conf. (ACC)*, May 2017, pp. 1462–1467.

EHSAN SHARAFIAN M. was born in Kermanshah, Iran, in 1994. He received the B.S. degree in mechanical engineering from the University of Tehran, in 2017, and the M.S. degree from the Amirkabir University of Technology (Tehran Polytechnique), in 2020. He is currently pursuing the Ph.D. degree in mechanical engineering with The University of Maine.

He is a Graduate Research Assistant with The University of Maine. His research is primarily focused on enhancing gait training for older adults through the use of haptic feedback systems, incorporating IMUs and vibromotors to improve their walking patterns, which may increase gait speed and stability. Additionally, he is developing health monitoring applications that can be deployed on smartphones utilizing deep learning features.

COLBY ELLIS received the B.S. degree in mechanical engineering with minors in math and robotics from The University of Maine, in 2023, where he is currently pursuing the M.S. degree in mechanical engineering with the Biorobotics and Biomechanics Laboratory.

His research has primarily focused on utilizing haptic feedback as a means of improving walking speed in older adults, specifically the design of smartphone-controlled haptic systems.

BABAK HEJRATI received the B.S. degree in mechanical engineering from Iran University of Science and Technology (IUST), in 2007, the M.S. degree in mechanical engineering from the K. N. Toosi University of Technology (KNTU), in 2009, and the Ph.D. degree in mechanical engineering from The University of Utah, in 2016.

He then completed a postdoctoral fellowship with Harvard University's Wyss Institute. In 2017, he joined the Department of Mechanical Engineering, The University of Maine, where he is currently an Associate Professor. He has secured research funding from NIH and DOE. He was a recipient of the NSF Faculty Early Career Development Award.